Chemical Engineering Journal 523 (2025) 168511

Contents lists available at ScienceDirect

Chemical Engineering Journal

journal homepage: www.elsevier.com/locate/cej

Photocatalytic disinfection of wastewater using peroxymonosulfate activated by pyrite, chalcopyrite and marcasite under solar irradiation

C. Gaye [a], P. García-Muñoz [a], J. Vazquez-Arenas [b], R.H. Lara [c], J. Rodríguez-Chueca [a,*]

[a] Department of Industrial Chemical & Environmental Engineering, Escuela Técnica Superior de Ingenieros Industriales, Universidad Politécnica de Madrid, C/José Gutiérrez Abascal 2, 28006, Madrid, Spain
[b] Centro Mexicano para la Producción más Limpia, Instituto Politécnico Nacional, Av. Acueducto s/n, Col. La Laguna Ticomán, Ciudad de México, 07340, Mexico
[c] Facultad de Ciencias Químicas, Universidad Juárez del Estado de Durango (UJED), Av. Veterinaria S/N, Circuito Universitario, 34120, Durango, DGO, Mexico

ARTICLE INFO

Keywords:
Photocatalysis
AOPs
Natural minerals-based catalysts
Enterococcus faecalis
Wastewater disinfection

ABSTRACT

This study investigates the photocatalytic potential of three natural iron-based minerals: pyrite, marcasite, and chalcopyrite for the inactivation of *Enterococcus faecalis* in simulated and real wastewater. Pyrite and marcasite (0.5 g/L) achieved complete bacterial inactivation within 90 and 30 min, respectively, while chalcopyrite only reached a 2.06 $\log_{10}$ reduction value (LRV) under the same conditions. The introduction of peroxymonosulfate (PMS) as an oxidant significantly improved disinfection kinetics, allowing a halving of the required mineral dosage. PMS activation by Fe^{2+} on mineral surfaces under solar irradiation generated highly reactive radicals ($SO_4^{\bullet-}$, $^{\bullet}OH$, and $O_2^{\bullet-}$), enhancing the overall oxidative capacity. Under optimized conditions (PMS/Pyrite/Solar and PMS/Marcasite/Solar), simultaneous removal of *E. faecalis* and tetracycline (TC) was demonstrated. TC removal efficiencies reached 98.99 and 88.90 % within 30 min, while complete bacterial inactivation occurred in 120 and 90 min, respectively. pH played a crucial role in system performance, since disinfection efficiency decreased at higher pH levels, though this effect was less severe in the pyrite-based system. The natural catalysts also showed a degree of pH self-regulation, reducing the need for chemical adjustment beneficial for practical deployment. Validation in real wastewater from a treatment plant near Madrid confirmed the systems' applicability, especially the PMS/Marcasite/Solar setup, which achieved full *E. faecalis* inactivation within 60 min along with a notable COD reduction. These results highlight the potential of solar-driven PMS activation using natural minerals for efficient, sustainable and low-cost wastewater disinfection.

1. Introduction

Each year, more than 360 km^3 of domestic and industrial wastewater is discharged into the environment worldwide. It is important to note that only 52 % of this enormous quantity is treated before being released into aquatic ecosystems [1]. These wastewater sources often contain numerous waterborne pathogens, including protozoa, viruses, and antibiotic-resistant bacteria [2,3], posing a significant risk to human health. This situation can have considerable consequences on public health, as these pathogenic organisms and organic compounds can enter the food chain through socio-economic activities related to aquatic ecosystems [4,5]. Consequently, the availability and quality of fresh water have become major challenges for the planet. This challenge is further complicated by the diverse composition of wastewater, which makes the inactivation of pathogenic microorganisms and the degradation of organic contaminants more difficult [6]. Wastewater recycling can be a viable option to reduce water pollution and increase its availability [7,8]. It has been widely reported that recycled water can be used in various sectors, such as agriculture, industry, and recreational and municipal purposes [9–11].

Spain is one of the first European countries to invest in water recycling, making it one of the top 10 countries in the world that recycle the largest amounts of wastewater [12]. Thanks to its high purification capacity and advanced expertise in this field, the amount of recycled wastewater was estimated at 457 hm^3/year (151 hm^3/year from direct reuse, and 306 hm^3/year from indirect reuse), as early as 2025. This process is based on Spain's national legislation on the reuse of recycled water (Royal Decree 1085/2024), aligned with the new European legislation (EU) 2020/741, which came into force in June 2023 [13]. In this context, disinfection is a crucial step to ensure better control of

* Corresponding author.
E-mail address: jorge.rodriguez.chueca@upm.es (J. Rodríguez-Chueca).

https://doi.org/10.1016/j.cej.2025.168511
Received 9 June 2025; Received in revised form 30 August 2025; Accepted 14 September 2025
Available online 15 September 2025

potentially infectious microorganisms before wastewater reuse.

Several conventional methods have already been developed for wastewater treatment before reuse [14–20]. Among these, chlorination, UV disinfection, ozonation and combinations of these techniques are commonly used. These treatment processes have often shown high efficiency in bacterial inactivation (*Escherichia coli*, *Enterococcus faecalis*, etc.) in water [21–23]. However, they have certain limitations, making it necessary to explore alternative approaches in this field of research.

Regarding chlorination, it can lead to the formation of toxic disinfection by-products (DBPs) and may contribute to the emergence of antibiotic-resistant bacteria, such as tetracycline-resistant strains [24]. UV disinfection has a strong elimination effect on microorganisms (MCs), but it can also produce intermediate products. When the intensity of UV-C irradiation is insufficient, it is likely to generate intermediate compounds such as small organic molecules (carboxylic acids, aldehydes, ketones, etc.), oxidized products, and incomplete degradation products (intermediates with some biological activity), which may still possess a certain degree of biotoxicity and interfere with the aquatic ecosystem [25–28]. Ozonation, on the other hand, has a high treatment cost, also produces DBPs, and lacks a long post-treatment effect, allowing microbial regrowth [29]. Thus, despite these advancements, microorganisms are not always effectively eliminated without generating secondary pollution in the form of DBPs. Furthermore, the way these bacteria respond to the stress imposed by disinfection techniques remains poorly understood and insufficiently documented. In this context, photocatalytic processes based on the activation of oxidants such as hydrogen peroxide (H_2O_2), peroxymonosulfate (PMS), and peroxydisulfate (PDS), in combination with solar radiation, present a promising alternative in the field of water and wastewater treatment [30]. These oxidants have been extensively activated through homogeneous or heterogeneous processes using various catalysts, including carbon-based materials (graphene oxide, biochar, etc.) [31], transition metals [25–28], magnetic nanomaterials [32], and α-MnO_2-based compounds [33]. These catalysts enable the generation of reactive oxygen species, such as hydroxyl radicals ($^{\bullet}OH$, 1.8–2.7 eV, 20 ns), sulfate radicals ($SO_4^{\bullet-}$, 2.5–3.1 eV, 30–40 μs), superoxide radicals ($O_2^{\bullet-}$, 2.4 eV), and singlet oxygen ($^1O_2$, 1.52 eV) [34–37]. Among these different oxidants, PMS appears to be the most beneficial to use. Not only does it can directly oxidize inorganic and organic compounds containing heteroatoms, but compared to H_2O_2 and PDS, it also seems to be the only oxidant that simultaneously produces both reactive oxygen species (ROS), $SO_4^{\bullet-}$ and $^{\bullet}OH$ [38,39]. This makes it highly relevant in sulfate radical-based advanced oxidation processes (SR-AOPs).

It is important to note that both homogeneous and heterogeneous activation processes have shown good efficiency in PMS activation [40], but they are often accompanied by drawbacks that must be considered. For example, in the case of homogeneous photocatalysts, the main challenge lies in the difficulty of recovering the catalyst for potential reuse, raising concerns about process viability [41]. In heterogeneous systems, although the recovery issue is mitigated, the high synthesis and production costs of photocatalysts pose a significant viability problem [42]. Therefore, the search for photocatalysts with good optical and structural properties while maintaining low production costs remains a key area of ongoing research.

In this context, the use of natural minerals containing transition metals, such as iron, can help reduce the cost of wastewater treatment processes. Iron sulfide (FeS_2) is one of the most widely distributed natural minerals in the Earth's crust. It exists in two crystalline forms: pyrite (cubic structure) and marcasite (orthorhombic structure) [43]. Pyrite, which is widely used, is characterized by a high content of iron ions (46.67 %) and sulfur (53.33 %), with a NaCl-type crystalline structure composed of Fe^{2+} and S_2^{2-} species [44]. The presence of Fe^{2+} facilitates PMS activation and the generation of reactive oxygen species (ROS). Meanwhile, S_2^{2-} ions play a crucial role as electron donors, accelerating the reduction of Fe^{3+} to Fe^{2+} and enhancing redox pair cycling within the reaction medium.

Copper-based minerals have been extensively explored as catalysts due to their ability to release metallic elements that function as reductants in the environment [45,46]. Among these, chalcopyrite ($CuFeS_2$), a bimetallic mineral composed of copper (35.78 %), sulfur (28.31 %), and iron (32.73 %), is one of the heterogeneous catalysts that has been tested in advanced oxidation processes (AOPs) for the degradation of organic contaminants in wastewater [47]. The catalytic mechanism of chalcopyrite typically proceeds through two main steps. Initially, low-valence Cu and Fe species on the mineral surface activate peroxides through electron transfer, facilitated by their variable oxidation states (Cu^+/Cu^{2+} and Fe^{2+}/Fe^{3+}) [48], leading to the generation of reactive free radicals and high-valence metal species. Subsequently, the high-valence metals react with reductive sulfur species present in the mineral, thereby regenerating the low-valence metal species and maintaining the catalytic cycle. As a result, mining can be used as a photocatalytic material in sulfate radical-based advanced oxidation processes (SR-AOPs) for wastewater treatment.

Several studies in the literature have focused on sulfate radical-based advanced oxidation processes (SR-AOPs), mainly for degrading organic compounds. For example, Wang et al. [49–51] investigated PMS activation using natural magnetite with hydroxylamine to enhance Rhodamine B degradation, achieving 61.82 % efficiency due to improved Fe^{2+}/Fe^{3+} redox cycling. Similarly, Zhu et al. [52] used a pyrite/persulfate system to degrade cyclohexanoic acid in petrochemical wastewater, reaching 90 % removal under optimal conditions (2 g/L pyrite, 4 mM persulfate). The study identified Fe^{2+} as active sites and emphasized Fe^{3+}–sulfur interactions in sustaining redox cycling and catalyst reusability. Yuan et al. [53] explored PMS activation by chalcopyrite to degrade ammonium dibutyldithiophosphate in wastewater, achieving 91.15 % removal in 80 min. $SO_4^{\bullet-}$, $^{\bullet}OH$, and $O_2^{\bullet-}$ radicals were identified as the main reactive species, while S^{2-} in $CuFeS_2$ helped reduce Fe^{3+} and Cu^{2+}, boosting efficiency.

However, very few studies have examined natural minerals as catalysts in SR-AOPs for water disinfection. To our knowledge, only three publications exist, two from our group. The first The first study [21] used ilmenite ($FeTiO_3$) and PMS under UV-A light to inactivate *E. faecalis* in distilled water, achieving complete inactivation in 120 min, with $SO_4^{\bullet-}$ and $^{\bullet}OH$ confirmed as key species. The second [54], also in collaboration with our team, used an atacamite-based ($Cu_2Cl(OH)_3$) PMS system under solar light to inactivate *E. faecalis* in simulated wastewater, reaching full inactivation in 30 min. The system generated various oxidizing species, notably $SO_4^{\bullet-}$ and $^{\bullet}OH$. The third study, by Wang et al. [25–28], assessed the disinfection of *Bacillus subtilis* and *E. coli* DH10H using a PMS and sodium percarbonate dual-oxidant system activated by natural pyrite. Inactivation values of 4.07 and 8.05 LRV were achieved, with $CO_3^{\bullet-}$ playing the main role, and $^{\bullet}OH$ and $O_2^{\bullet-}$ contributing to a lesser extent.

This study fills a notable gap in the scientific literature, as no previous work has reported the use of natural mineral-based catalysts for SR-AOPs in water disinfection. It investigates three naturally occurring minerals rich in iron, sulfur, and copper as efficient, low-cost photocatalysts for activating peroxymonosulfate (PMS) in both simulated and real wastewater. Unlike conventional synthetic catalysts, which often rely on expensive metal precursors and require chemical modification, these minerals can be used directly, offering a simpler, more sustainable alternative. Importantly, such materials could be sourced from mining residues, adding value to industrial waste streams while reducing overall treatment costs. This approach enables simultaneous degradation of organic pollutants and inactivation of microorganisms, making it a promising, scalable, and environmentally friendly solution for advanced water treatment.

The objective of this study is, first, to characterize the selected natural minerals. In a second phase, these minerals will be applied as photocatalysts for PMS activation under solar irradiation, aiming at the inactivation of *Enterococcus faecalis*. We also plan to investigate the recovery and reuse of the catalysts, as well as the influence of various

parameters such as catalyst dose, PMS concentration, pH, matrix effect. The study of tetracycline (TC) removal under conditions optimized for *E. faecalis* inactivation will also be carried out. Finally, the process will be applied to a real wastewater matrix.

2. Materials and methods

2.1. Mineral samples and characterizations

Massive samples of marcasite (FeS_2) were purchased from Excalibur Mineral Corp (Charlottesville, VA, USA), while massive samples of pyrite (FeS_2) were obtained from Charcas mining unit (San Luis Potosí, SLP). Additionally, chalcopyrite ($CuFeS_2$) samples were adquired from at Zacatecas, Zac (Central Mexico). Coupons of pyrite and marcasite were used to fabricate mineral electrodes (exposed surface area equals 1 cm^2), which were polished to a mirror-like appearance prior to the electrochemical characterization. These measurements were conducted using a Biologic SP-150 potentiostat/galvanostat. A Pyrex™ glass three-electrode cell was used to carry out these measurements with pyrite or marcasite specimens, and a graphite rod of high purity as working and counter electrodes, respectively. In this configuration, a saturated sulfate electrode was employed as reference (0.615 V vs. SHE) in a 0.1 M $HClO_4$ (JT Baker, analytical grade reagent) electrolyte. In all cases, a scan rate of 20 mV s^{-1} was used to perform voltammetry experiments, starting at the open circuit potential (OCP) with a resting of 60 s.

2.2. Structural and surface analysis of pyrite and marcasite

The structural characteristics of the mineral samples (as-received) was analyzed by X-ray diffraction (XRD) under a configuration Bragg-Brentano, in a PANalytical Empyrean equipment using a Co K_α radiation source (λ =1.7905 Å), while the morphology and elemental composition of the minerals was evaluated by scanning electron microscopy coupled to Energy-dispersive X-ray spectroscopy (SEM-EDS) using a secondary electron detector in a Carl Zeiss SIGMA 300 VP microscope at 15 kV.

2.3. Water matrices

To facilitate the application of the process to a real wastewater sample, all experiments in this study were conducted using a simulated wastewater matrix, specifically designed to replicate the characteristics of secondary effluent from wastewater treatment plants. The selection of this matrix was based on the need to maintain consistent physicochemical and biological attributes, closely resembling real wastewater after secondary treatment, thereby ensuring the reproducibility of the experiments. The simulated wastewater matrix consisted of urea (Sharlau; 6 mg·L^{-1}), meat peptone (Sharlau; 32 mg·L^{-1}), meat extract (Sharlau; 22 mg·L^{-1}), sodium chloride (Sharlau; 7 mg·L^{-1}), calcium chloride (Sharlau; 4 mg·L^{-1}), potassium dihydrogen phosphate (Sharlau; 28 mg·L^{-1}), and magnesium sulfate (Sharlau; 2 mg·L^{-1}). Additionally, a real wastewater sample was collected from a wastewater treatment plant (WWTP) located in the center of Spain. The full physicochemical characterization of both matrices is summarized in Table 1.

Table 1
Physicochemical and biological characterizations of both water matrices before treatment.

Parameter (units)	Simulated wastewater	Real wastewater
pH	5.30	5.72
ORP (mV)	33.00	36.00
Conductivity (µS/cm)	82.30	149.30
Turbidity (NTU)	< 0.10	7.08
COD (mg O_2/L)	60.00	31.00
Total Aerobic Microorganisms (CFU/mL)	–	4666.66
E. faecalis (CFU/mL)	–	200.00

2.4. Chemicals reagents

In addition to the reagents listed in section 2.3 for the preparation of simulated wastewater samples, other reagents were also required to successfully carry out the experiments described in this manuscript. Peroxymonosulfate (PMS; HSO_5^-; Sigma-Aldrich) was used as an oxidant within a concentration range of 0.001 to 1 mM. Additionally, hydrochloric acid (HCl; Labkem) and sodium hydroxide (NaOH; Panreac) were used for pH adjustments. Methanol (MeOH; CH_4O; Sigma-Aldrich), tert-butanol (TBA; $C_4H_{10}O$; Sigma-Aldrich), trichloromethane ($CHCl_3$; Labkem), and furfuryl alcohol (FFA; $C_5H_6O_2$; Sigma-Aldrich) were used as radical scavengers at concentrations ranging from 10 to 50 mM. MeOH and tert-TBA were selected due to their differing reactivity with hydroxyl ($^{\bullet}OH$) and sulfate ($SO_4^{\bullet-}$) radicals. While MeOH effectively quenches both radicals, TBA selectively inhibits $^{\bullet}OH$ activity. $CHCl_3$ was used as a scavenger for superoxide radicals ($O_2^{\bullet-}$), and to assess the potential role of singlet oxygen ($^1O_2$), furfuryl alcohol FFA was employed.

2.5. Microbiological analysis

For microbiological analysis, simulated wastewater samples were intentionally contaminated with an *Enterococcus faecalis* strain (ATCC 29212, Scharlab). As highlighted in the introduction, *E. faecalis* was selected as the bacterial contaminant due to its Gram-positive nature and higher resistance to treatment compared to other bacterial indicators, such as *Escherichia coli* (a Gram-negative bacterium) [55].

To prepare the bacterial culture, a fresh liquid culture of *E. faecalis* was grown in Luria-Bertani (LB) nutrient broth (Sharlau) for 24 h at 37 °C in a shaker incubator. The bacterial suspension was then centrifuged at 4,500 rpm for 15 min to separate the cells, which were subsequently resuspended in a sterile 0.9 % NaOH saline solution.

For the experimental setup, the bacterial suspension was diluted in a 100 mL reactor to achieve an initial concentration of 10^6 CFU/mL. Samples were collected at regular time intervals, serially diluted tenfold in the same 0.9 % NaOH solution, and plated onto Slanetz & Bartley medium (Condalab) using both the drop plate method and spread plate method. To assess bacterial survival, colony-forming units (CFUs) were counted after incubating the plates at 37 °C for 48 h. The detection limit (DL) was determined using the spread plate method and it was estimated at 10 CFU/mL.

2.6. Tetracycline determination

Tetracycline (TC) determination was measured in HPLC (Agilent Technologies, Model 1100 Series), with a C-18 column and a 276 nm UV detector. The mobile phase consisted of 2 % acetic acid and Acetonitrile with a volume ratio of 90:10. The inactivation of *E. faecalis* and the degradation of tetracycline (TC) under the optimal conditions of the various processes were carried out in a batch reactor containing 100 mL of simulated wastewater, enriched with 10^6 CFU/mL of *E. faecalis* and 10 ppm of TC (Sigma-Aldrich).

2.7. Experimental setup

The inactivation of *E. faecalis* through the various photocatalytic processes studied was carried out in a batch reactor containing 100 mL of simulated wastewater enriched with *E. faecalis*. All experiments were conducted with a concentration of 10^6 CFU/mL of *E. faecalis*. The 10 ppm of tetracycline (TC) was added to the reactor only during the simultaneous removal experiments, performed under optimal conditions. A range of catalysts doses from 50 mg·L^{-1} to 500 mg·L^{-1} was added to the reactor, combined as needed with PMS concentrations

ranging from 0.01 to 1 mM. The experiments were conducted in 250 mL beakers under continuous stirring at an average speed of 500 rpm. All photocatalytic experiments were performed using a solar simulator (SUNUTEST CPS Hereaus) equipped with a 1500 W xenon lamp. This simulator has a spectral distribution where approximately 0.5 % of the emitted photons have a wavelength below 320 nm (UV-B) and about 5 to 7 % fall within the 300–400 nm range (UV-A). Additionally, the device is equipped with an air-cooling system and a support with water inlet and outlet, ensuring that the reaction temperature remains stable between 25 and 30 °C.

2.8. Bacterial inactivation kinetics

To compare bacterial inactivation in the different processes studied, a kinetic study was conducted using the pseudo-first-order model described by Eq. (1):

$$log\frac{N_t}{N_0} = K_{obs}\cdot t \quad (1)$$

where N_0 represents the bacterial concentration before irradiation, N_t represents the concentration of viable bacteria after irradiation at a given time, t is the irradiation time, and K_{obs} is the first-order inactivation constant. Thus, using the K_{obs} value, a comparison of the two processes involving different catalysts was conducted. The synergistic effect of each process was studied by determining the synergistic factor between the oxidant, the catalyst, and solar radiation, according to the model described by Eq. (2) [56].

$$S = \frac{K_{123}}{((K_1+K_2+K_3)+(K_{12}-K_1-K_2)+(K_{23}-K_2-K_3)+(K_{31}-K_3-K_1))} \quad (2)$$

In this formula, the subindex 1 represents PMS, the subindex 2 represents the catalyst, and the subindex 3 represents the solar radiation.

2.9. Determination of Chemical Oxygen Demand (COD)

The Chemical Oxygen Demand (COD) was determined using a HI83399 multiparameter photometer (Hanna Instruments), following the USEPA-approved Method 410.4. This method is based on the oxidation of organic compounds present in the sample by dichromate ions ($Cr_2O_7^{2-}$) in a strongly acidic medium (H_2SO_4), in the presence of a catalyst and under reflux heating conditions. Specifically, a measured volume of the sample was introduced into a reaction tube containing a mixture of sulfuric acid and potassium dichromate. The sealed tubes were then heated at 150 °C for 2 h to ensure complete oxidation of the organic matter. After cooling, the amount of residual dichromate or the concentration of chromium ions (Cr^{3+}) formed was quantified by direct colorimetric analysis using the photometer. The COD values were expressed in mg $O_2\cdot L^{-1}$, within a range of 0 to 150 mg $O_2\cdot L^{-1}$, with a reading precision of 5 mg $O_2\cdot L^{-1}$ at 25 °C, corresponding to the amount of oxygen consumed during the chemical oxidation of organic substances. All analyses were performed duplicate, and blanks were included for each series to ensure the accuracy and reliability of the results.

3. Results and discussions

3.1. Structural, textural and electrochemical characterizations

Fig. 1 shows experimental XRD of the natural minerals (as-received) under a configuration Bragg-Brentano. The indexing of these experimental data reveals that the pyrite sample is mainly composed of FeS_2 (PDF card No. 96-722-8543) with space group Pa_{-3}, presenting traces of Fe_3S_4 (Greigyte, PDF card No. 96-900-0124) with space group P_{121}/n_1. This type of impurities is a typical inclusion presented in natural minerals due to the geological activity of ores. On the other hand, the Marcasite sample is accurately identified as this crystalline structure (PDF card No. 96-900-0006) with space group *Pnnm,* and pyrite as minor impurity. Finally, Chalcopyrite is mainly composed of $CuFeS_2$ (PDF card

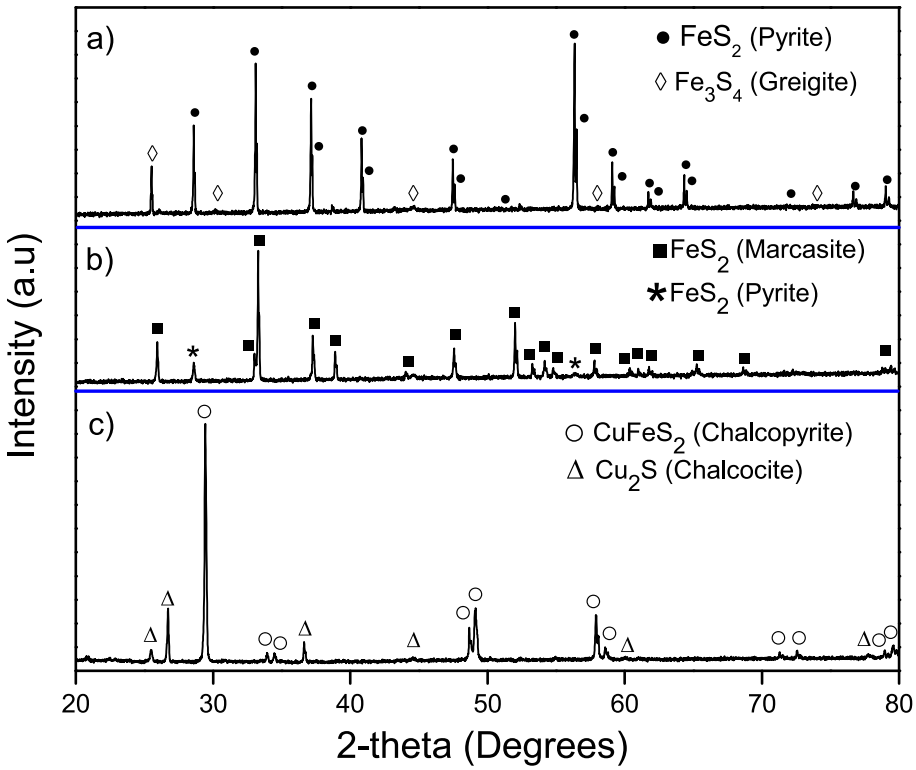

Fig. 1. Experimental X-ray diffractograms collected from the as-received natural mineral samples: a) pyrite; b) marcasite; c) chalcopyrite.

No. 96-210-4743) with space group I_{42d} and presenting traces of Cu_2S (Chalcocite, PDF card No. 96-900-5551, space group $P_{21/n}$.

Fig. 2 describes micrographs collected with natural mineral samples. A comparison of the average particle sizes of the two minerals indicates that the particle diameter is smaller in the case of marcasite and chalcopyrite (~40–70 nm) compared to pyrite (~70–90 nm). Both samples are apparently homogeneous in size, and the morphology displayed by marcasite and chalcopyrite is much rougher than that displayed by pyrite. Elemental analysis by EDS performed on the samples (Figs. S1, S2 and S3 in Supplementary Material) reveals that the marcasite mineral presents a stoichiometry close to FeS_2 based on the atomic composition, but with many impurities at the trace level, except for the elemental O content. Something similar occurs with chalcopyrite, in which traces of other metals such as Cu and Au are also found. This composition stands out although it presents a lower wt% than Fe or S, which could indicate the presence of secondary Fe oxides/hydroxides resulting from its oxidation in the environment. However, pyrite does not present significant trace elements, including the absence of elemental O, which contributes to a better preservation of its FeS_2 stoichiometry. Presumably, this modification between the surface composition of pyrite and marcasite could modify their catalytic activity, despite their similar crystal lattices and atomic composition. The analyses in Figs. 1 and 2 confirm the presence of natural phases of pyrite and marcasite that can be used for the application described below.

On the other hand, the determination of specific surface area is not commonly performed, as pristine minerals typically exhibit low or negligible porosity and therefore present smooth surfaces unless subjected to a pretreatment. According to the literature, marcasite and pyrite exhibit typical BET-specific surface area ranges of 0.5 to 4.5 $m^2 \cdot g^{-1}$ [57–59], and 0.05 to 1.2 $m^2 \cdot g^{-1}$ [60,61], respectively. The authors have conducted surface area measurements (N_2 adsorption-desorption isotherms not shown), finding values of 0.49 and 2.70 $m^2 \cdot g^{-1}$ for the pristine pyrite and marcasite samples used in this study, respectively. These results suggest that the activity of these minerals will not rely on porous media (i.e. specific surface area).

Fig. 3 shows cyclic voltammograms of pyrite and marcasite, initiated from the OCP (open circuit potential) in the positive direction. These experiments were conducted in 0.1 M $HClO_4$ (pH 2) under stagnant conditions. This comparison was performed to determine the anodic and cathodic regions of both minerals, and analyzing their activity based on the current density reached. In general, the marcasite has a lower oxidation activity compared to pyrite (Fig. 3). In the positive region of this mineral, a scant oxidation process identified as O1, was detected. However, an abrupt increase of current was observed toward more positive potentials in the anodic region (Fig. 3, O2 process). The magnitude of the current associated with the O2 contribution makes the O1 appear negligible; indicating that O1 involves a low oxidation reaction. This indicates minimal changes in surface mineral structure. In contrast, the oxidative behavior of pyrite was considerably more active, with an initial process O1, which again presents a lower oxidation

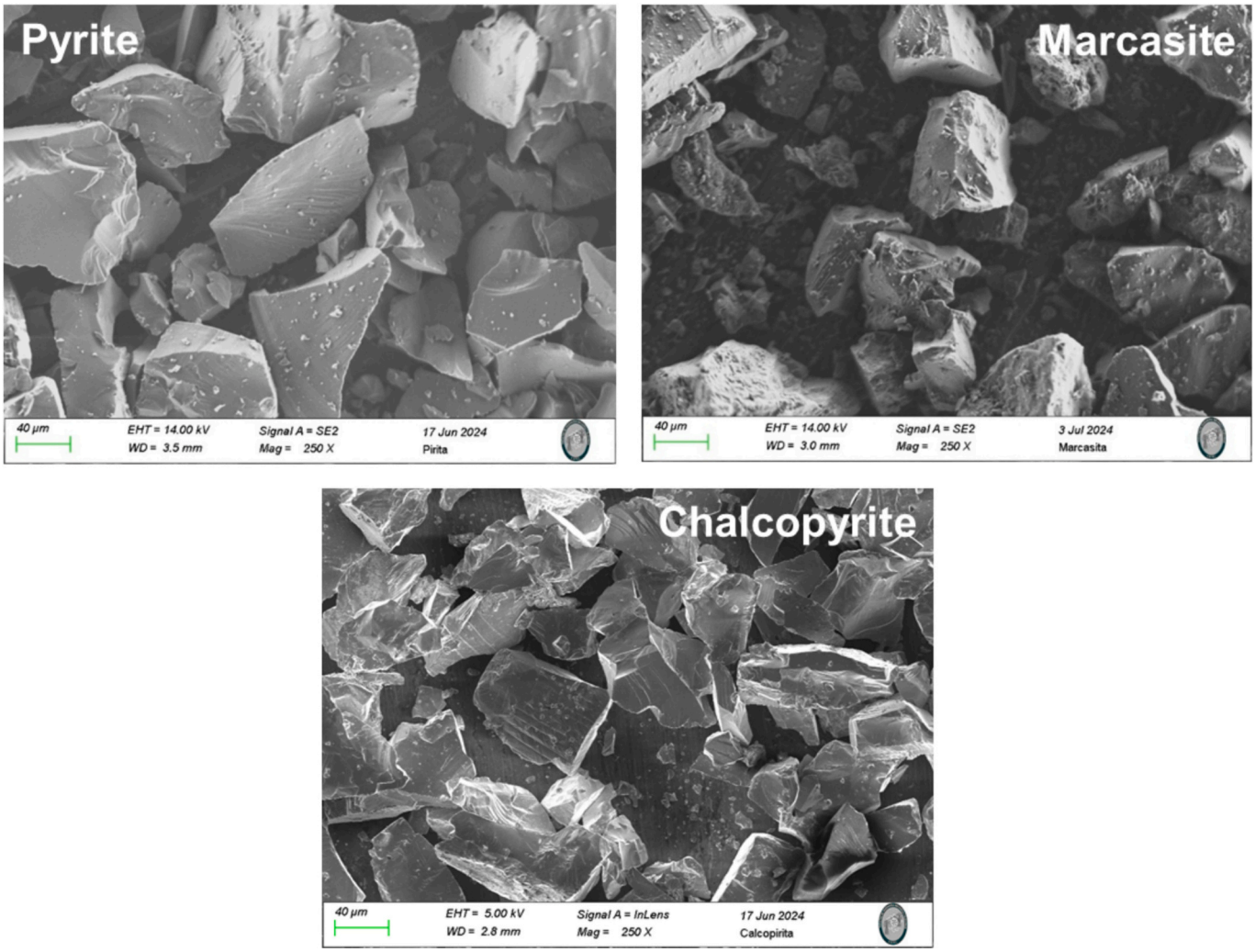

Fig. 2. SEM micrographs collected from the as-received natural mineral samples.

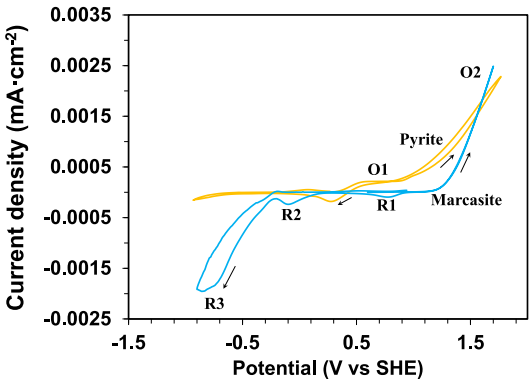

Fig. 3. Cyclic voltammograms of pyrite and marcasite initiated on the positive direction using scan rates of 20 mV s^{-1} in 0.1 M $HClO_4$. Stagnant conditions at 25 °C.

contribution compared to O2, which shows a steep current increase (Fig. 1) [62]. When the scan is inverted into the cathodic region, two minor reduction processes R1 and R2 appear, which may be related to the reduction of iron oxides and reduced sulfur phases such as polysulfides (S_n^{2-}). Not surprisingly, the reduction of marcasite is more important due to the presence of Fe oxide phases as detected in the EDS elemental analysis (Supplementary material), and perhaps the contributions arising from reduction processes associated with polysulfides or mixtures of sulfur (e.g. S^0/S_n^{2-}). These inputs are not observed in the pyrite, which did not present a significant number of oxides in the EDS evaluation. These results suggest that the activity of pyrite is greater at low/medium overpotentials of mineral oxidation, but it is slower as the potential becomes either more positive or negative. An opposite behavior is observed for marcasite.

UV–Vis diffuse reflectance spectra (DRS) of pyrite and marcasite were collected, as shown in Fig. S4a in Supplementary Material, revealing significant absorption for both minerals in approximately 300–600 nm (pyrite) and 300–720 nm (marcasite), with stronger overall

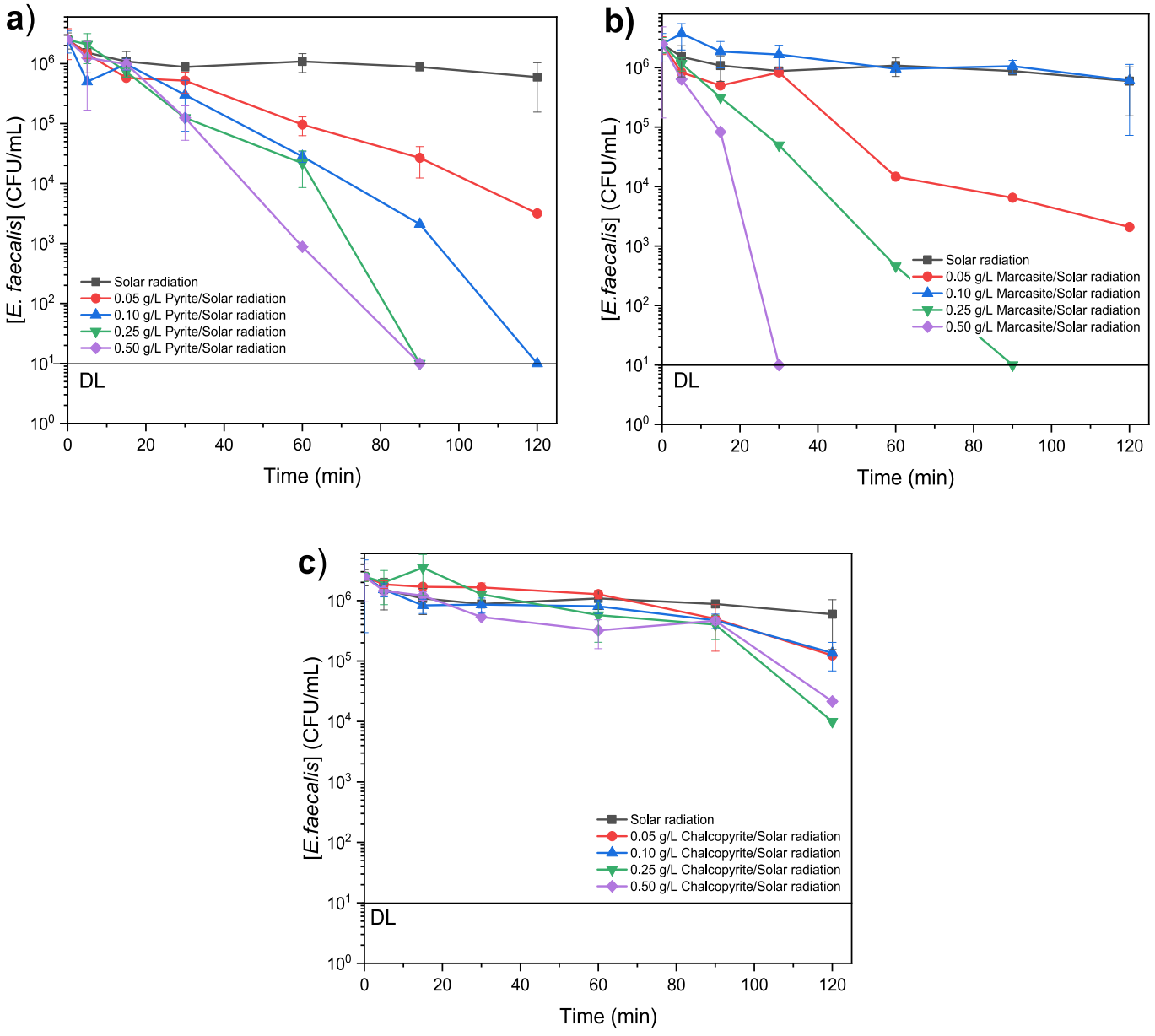

Fig. 4. *E. faecalis* inactivation by the photocatalytic effect of minerals under solar radiation a) Pyrite, b) Marcasite and c) Chalcopyrite. [Catalyst] = 0.05–0.5 $g{\cdot}L^{-1}$; Radiation intensity = 16.07 Wm^{-2}; unadjusted pH.

light absorption observed for pyrite. Based on these data, Tauc plots ([F(R)·$h\nu$]^2 vs $h\nu$, Fig. S4b) were evaluated using the Kubelka–Munk function (powder analysis) assuming direct-allowed transitions, yielding band-gap values of 2.8 and 1.2 eV for pyrite and marcasite, respectively. The marcasite value is very close to that reported in the literature, 0.927 eV [63], whereas the band gap of pyrite has been described over a broad range from 1.5 to 3.2 eV for cubic and spherical pyrite, respectively [64,65]. Presumably, this parameter could be influenced by a significant *Greigite* contribution in the pyrite mineral, as indicated by the XRD analysis shown in Fig. 1.

In general, flat-band potentials lie ~0.1–0.3 eV more negative than the valence band in p-type semiconductors (e.g. marcasite), and ~ 0.1–0.3 eV more positive than the conduction band in n-type semiconductors (e.g. pyrite). Under this premise, flat-band potentials for pyrite and marcasite determined experimentally in the literature of 0.727 and 2.757 eV, respectively [63], which along with the band gaps evaluated in Fig. S9b, enabled to estimate the following energetic bands, $E_{VB}^{pyrite} = 3.527$ eV and $E_{CB}^{marcasite} = 1.557$ eV. These calculated values indicate a suitable band alignment to catalyze PMS activation by Fe^{2+} on both mineral surfaces.

3.2. Photocatalytic activity of minerals

Pyrite, marcasite and chalcopyrite were initially tested as photocatalysts to assess their effectiveness in inactivating *E. faecalis* under solar irradiation (Fig. 4). As can be observed in Fig. 4, in the absence of solar radiation, the removal efficiencies obtained were 0.452 $\log_{10}$ ($\log_{10}$ reduction value, LRV) and 0.845 LRV for pyrite and marcasite (Fig. S5, and Table S2 supplementary material), respectively, after 120 min of treatment. These results indicate that both minerals have low antibacterial properties and ability to adsorb *E. faecalis*. However, as shown in Fig. 4a and b, the *E. faecalis* inactivation rate was found to be proportional to the catalyst dose, both for the Pyrite/Solar and Marcasite/Solar systems. With the highest catalyst dose (0.5 g·L^{-1}), the detection limit was reached after 90 and 30 min of treatment, respectively, for the pyrite/Solar and marcasite/Solar systems. This increase in *E. faecalis* inactivation with increasing catalyst dose can be attributed to the continuous generation of ROS via a photocatalytic process, facilitated by the ongoing dissolution of Fe^{2+} at the surface of FeS_2 (see Table S1 for Supplementary Material) as well as the cycling of Fe^{2+}/Fe^{3+} [17,18]. Indeed, pyrite (E° = 0.95 eV) and marcasite (E° = 1.1 eV) behave as semiconductors by absorbing light to generate electrons and photo-induced holes (h^+) [66]. With the h^+/e^- pair, oxygen molecules in the medium acquire electrons to produce H_2O_2, inducing a photocatalytic process (Eqs. 3–8 that generates the radicals $^{\bullet}OH$ and $O_2^{\bullet-}$, which can effectively degrade *E. faecalis*. These radicals can damage and destroy the bacterial cell membranes, leading to a significant reduction in the bacterial population observed.

$$FeS_2 + h\nu \rightarrow FeS_2(h^+ + e^-) \quad (3)$$

$$h^+ + H_2O \rightarrow OH^- + H^+ \quad (4)$$

$$h^+ + OH^- \rightarrow OH^{\bullet} \quad (5)$$

$$e^- + O_2 \rightarrow O_2^{\bullet-} \quad (6)$$

$$2e^- + 2H^+ + O_2 \rightarrow H_2O_2 \quad (7)$$

$$\equiv Fe^{2+} + H_2O_2 \rightarrow \equiv Fe^{3+} + OH^{\bullet} + OH^- \quad (8)$$

Similar results were recently reported by *García-Muñoz* et al. [67] when studying the inactivation of *E. faecalis* using a Fe_2O_3-$mTiO_2$/PMS/Solar system. With the same catalyst concentration (0.5 g·L^{-1}), complete *E. faecalis* elimination was achieved after 90 min of treatment. They attributed this result to a photocatalytic process involving the generation of $^{\bullet}OH$ and $O_2^{\bullet-}$radicals. This finding supports the photoactivity of both pyrite and marcasite through a photocatalytic inactivation process, characterized by the in-situ production of H_2O_2 via oxygen molecules acting as electron acceptors, as described in the above-mentioned equations. Although both crystalline forms allowed complete bacterial inactivation, it is important to note that marcasite required a shorter treatment time to eliminate the bacterial population. Given that pyrite has a narrower band gap than marcasite and greater structural stability, the superior photocatalytic performance of marcasite can be attributed to its orthorhombic morphology, which may narrow the FeS_2 band gap, thus facilitating the separation of photogenerated electron-hole pairs (e^-/h^+), accelerating the Fe^{3+}/Fe^{2+} redox cycle, and enhancing $^{\bullet}OH$ radical generation [68]. *Zhang* et al. [69] similarly reported that the photocatalytic effects of pyrite during the photo-Fenton degradation of sulfadiazine varied depending on the mineral's morphology. They explained that differences in crystal planes and sulfur vacancies caused variations in photocatalytic synergies across the different FeS_2 morphologies studied.

Like pyrite and marcasite, chalcopyrite also exhibited poor *E. faecalis* inactivation capacity in the dark, achieving an inactivation rate of approximately 0.079 LRV (Fig. S5 in supplementary information). However, under solar irradiation, chalcopyrite followed the same trend observed with pyrite and marcasite (Fig. 4c), although with significantly lower inactivation efficiency, not exceeding 2 LRV even at the optimal catalyst dose (0.25 g·L^{-1}).

This relatively low catalytic activity of chalcopyrite may partly be due to the rapid recombination of photogenerated charges. Indeed, chalcopyrite has a smaller band gap (~0.6–0.7 eV), which favors electron-hole recombination, thus reducing photocatalytic efficiency despite its good light absorption capacity. The structural differences between marcasite and pyrite, as well as the narrow band gap of chalcopyrite, significantly influence their electronic properties and photocatalytic performance.

3.3. Baseline operating condition

To optimize the photocatalytic inactivation process of *E. faecalis* and enhance the production of reactive species such as $SO_4^{\bullet-}$, the combination of the minerals with PMS under solar irradiation was tested. It is worth mentioning that several studies on the combination of PMS with light sources such as UV-C, UV-A, and solar radiation have been extensively carried out by our research group [13,21,30,67,70]. In all these cases, the PMS/UV and PMS/Solar systems demonstrated sufficiently high oxidation capacities to eliminate an initial *E. faecalis* concentration of 10^6 CFU/mL within just a few minutes of treatment.

Therefore, to optimize PMS dosage, different PMS concentrations

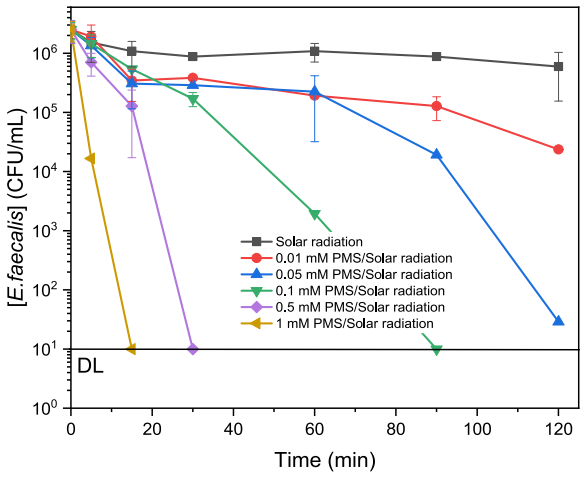

Fig. 5. *E. faecalis* removal by PMS/Solar system with different doses of PMS. Radiation intensity 16.07 W m^{-2}, at unadjusted pH.

were tested under solar irradiation alone, as shown in Fig. 5. The range of PMS concentrations evaluated varied between 0.001 and 1 mM. A direct correlation between increased PMS concentration and bacterial inactivation was observed, with the detection limit being achieved at PMS concentrations of 0.1, 0.5, and 1 mM after 120, 30, and 15 min of treatment, respectively. This strong inactivation capability of the PMS/Solar process can be attributed to the generation of $SO_4^{\bullet-}$ and $^{\bullet}OH$ radicals resulting from PMS decomposition, as illustrated in Eq. 9. Consequently, any PMS concentration above 0.05 mM was excluded from further studies, even though concentrations between 0.5 and 3 mM have recently been employed in other works [71–74].

Thus, the results presented in Fig. 5 will serve only as a reference for the individual effects of each reactant that will later be combined in the PMS/Mineral/Solar processes.

$$HSO_5^- + h\nu \rightarrow SO_4^{\bullet-} + OH^{\bullet} \quad (9)$$

3.4. PMS/mineral/solar system optimization

To enhance the photocatalytic capacity of both photocatalysts and reduce their required dosages, a combination with PMS was tested using different loads of the three different minerals, acting as catalysts. Fig. 6 shows the inactivation results of *E. faecalis* obtained for catalyst doses ranging from 0.05 to 0.5 g·L^{-1}. It was observed that increasing the load of pyrite (Fig. 6a) and marcasite (Fig. 6b) had a positive effect, with the inactivation efficiency of *E. faecalis* progressively improving as the dose increased from 0.05 to 0.25 g·L^{-1}. At this optimal load (0.25 g·L^{-1}), complete inactivation was achieved within 60 and 30 min for the PMS/Pyrite/Solar and PMS/Marcasite/Solar processes, respectively.

Compared to the results obtained from the pure photocatalytic systems (Pyrite/Solar and Marcasite/Solar), it is notable that while all four systems eventually achieved the detection limit, the required treatment times were significantly reduced in the PMS-assisted systems, from 90 min (without PMS) to 60 and 30 min with PMS, for the same catalyst

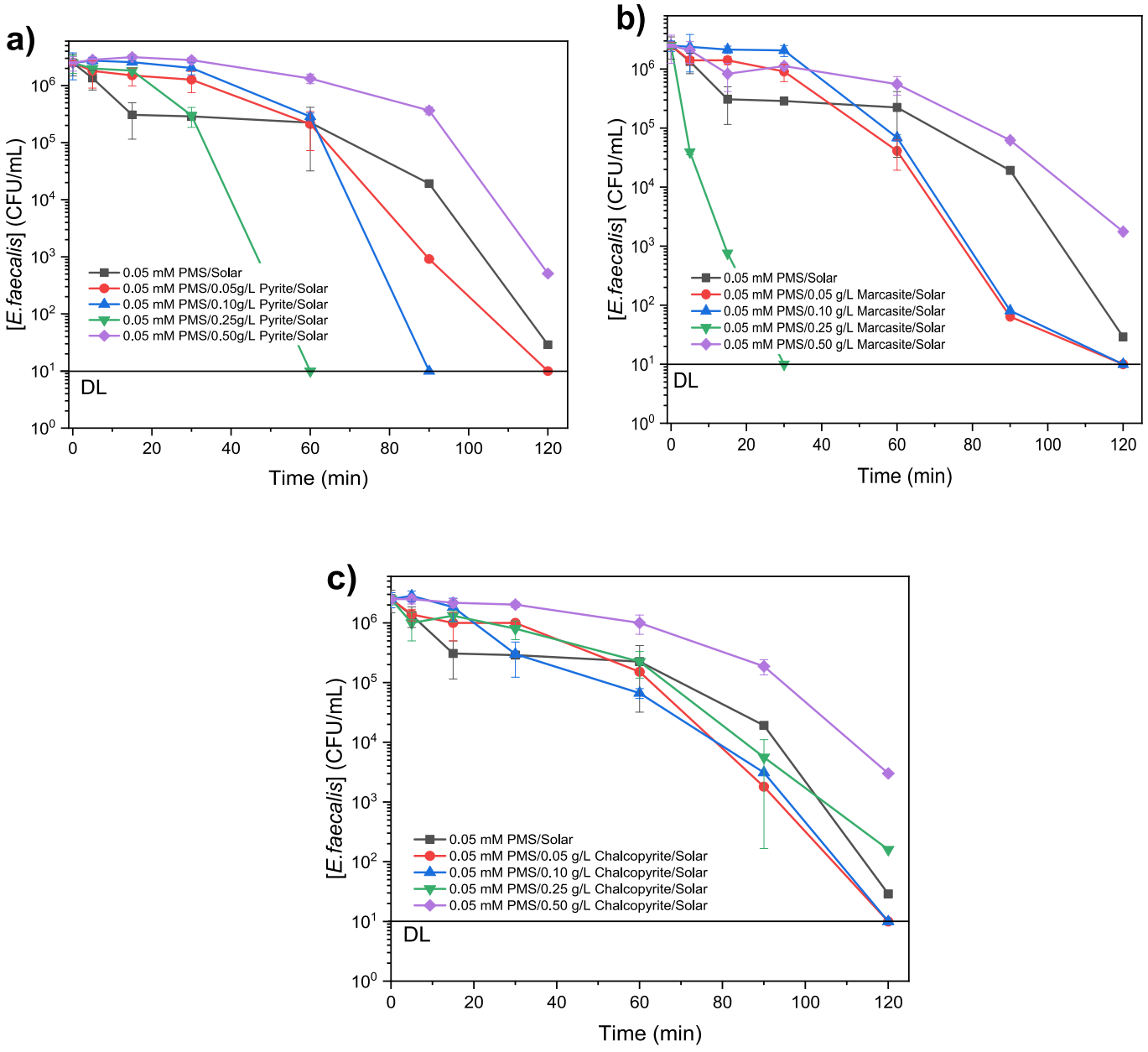

Fig. 6. Optimization of a) Pyrite, b) Marcasite, and c) Chalcopyrite loads for *E. faecalis* inactivation under solar irradiation. [PMS] = 0.05 mM, radiation intensity 16.07 W m^{-2} at unadjusted pH.

dose (0.25 g·L^{-1}). Furthermore, considering that the combination of 0.05 mM PMS with solar irradiation alone did not reach the detection limit even after 120 min, it can be suggested that, in addition to the light-driven activation of PMS, a catalytic activation is initiated by Fe^{2+} ions released from the surface of pyrite and marcasite [66], promoting the generation of $SO_4^{\bullet-}$ and $^{\bullet}OH$ radicals (Eqs. 10 and 11).

Similar results were previously reported by *García-Muñoz* et al. [21], who studied the inactivation of *E. faecalis* through the Ilmenite/PMS/UV-A process. They attributed PMS activation not only to the effect of light but also to the catalytic action of Fe^{2+} ions released from the surface of ilmenite (a mineral based on iron and titanium).

$$\equiv Fe^{2+} + HSO_5^- \rightarrow \equiv Fe^{3+} + SO_4^{\bullet-} + OH^- \quad (10)$$

$$\equiv Fe^{2+} + HSO_5^- \rightarrow \equiv Fe^{3+} + SO_4^{2-} + {}^{\bullet}OH \quad (11)$$

In such processes, the regeneration of Fe^{2+} plays a crucial role by maintaining the system's reactivity and ensuring a continuous supply of Fe^{2+} through the ongoing reduction of Fe^{3+} back to Fe^{2+} (Eq. 12). This active Fe^{2+}/Fe^{3+} cycling at the catalyst surface sustains the continuous generation of ROS. *Rodríguez-Chueca* et al. [70] reported that Fe^{3+} can participate in a regenerative catalytic cycle under light irradiation, where Fe^{3+} is photoreduced to Fe^{2+}. This process enabled the effective and sustained activation of PDS and sufficient production of $SO_4^{\bullet-}$ radicals, leading to the successful inactivation of *E. coli*.

$$\equiv Fe^{3+} + e^- \rightarrow \equiv Fe^{2+} \quad (12)$$

From this perspective, pyrite and marcasite, which contain high amounts of iron and sulfur, offer a significant advantage over the use of traditional transition metals or metal oxides as photocatalysts. This phenomenon appears to be more pronounced and active in the case of marcasite, as the shorter treatment time suggests a faster generation of ROS.

However, when the catalyst dose was doubled (0.5 g·L^{-1}), a drastic decrease in the *E. faecalis* inactivation efficiency was observed, with final LRV of 3.69 and 3.15 at 120 min for the PMS/Pyrite/Solar and PMS/Marcasite/Solar processes, respectively. This inhibition of the photocatalytic process can be attributed to the excess generation of electrons (e^-), holes (h^+), and Fe^{2+} after light absorption by pyrite and marcasite, as well as a screening effect that prevents effective PMS decomposition into reactive radical species. An overabundance of e^- and h^+ can also induce rapid recombination reactions between ROS and PMS, leading to the formation of radicals with lower oxidation potential such as $SO_5^{\bullet-}$ ($E^{\circ} = 1.1$ V) (Eqs. 13–15) [70,75].

Overall, this phenomenon reduces the availability of highly reactive species and, consequently, the efficiency of the PMS/Pyrite/Solar and PMS/Marcasite/Solar processes. Therefore, to achieve better performance in terms of reagent consumption and treatment time, a catalyst dose of 0.25 g·L^{-1} was selected for the remainder of the study.

$$SO4^{\bullet-} + HSO_5^- \rightarrow SO_5^{\bullet-} + HSO_4^- \quad (13)$$

$$\equiv Fe^{2+} + SO_4^{\bullet-} \rightarrow \equiv Fe^{3+} + SO_4^{2-} \quad (14)$$

$$\equiv Fe^{2+} + h^+ \rightarrow \equiv Fe^{3+} \quad (15)$$

While the combination of chalcopyrite with PMS under solar irradiation showed worst results compared to pyrite and marcasite in terms of water disinfection (Fig. 6c). In this case, the detection limit was reached after 120 min of treatment using an optimal chalcopyrite dose of 0.05 g·L^{-1}. Beyond this dosage, a decrease in inactivation efficiency was observed. Two important observations can be made: although the DL was reached, the treatment time required was significantly longer compared to the processes using pyrite and marcasite. Additionally, when compared to the Chalcopyrite/Solar process, it appears that the addition of PMS had a positive effect. However, this improvement is likely due primarily to the photocatalysis of PMS under solar irradiation, which leads to the generation of reactive species, as the PMS/Solar process alone yielded nearly the same inactivation results after 120 min. This further confirms the low photocatalytic activity of chalcopyrite, which can be attributed to the rapid recombination of charge carriers before they participate in photocatalytic reactions [49–51,76]. Thus, the strong semiconductor character developed during the oxidation of chalcopyrite, due to the formation of elemental sulfur, acts as a barrier to effective charge release, thereby hindering PMS activation. This hypothesis can be further supported by the study conducted by Bai et al. [77] on the in situ electrochemical leaching of chalcopyrite. They concluded that the leaching products, such as elemental sulfur mixed with iron-depleted sulfides, led to the passivation of the chalcopyrite surface.

It is also worth noting that the optimal dose used in this system is much lower than those for the other two catalysts, indicating that excess chalcopyrite is not favorable for ROS production and *E. faecalis* inactivation. A high dose may lead to negative effects such as limited diffusion, inactive surface sites, aggregation, or non-productive radical consumption, ultimately reducing the process efficiency. Similar findings have been reported in the literature. *Barhoumi* et al. [78] for instance, investigated the effect of chalcopyrite dosage in a photo-Fenton process for tetracycline degradation. These authors showed that increasing the amount of chalcopyrite was detrimental to the degradation kinetics of tetracycline.

Considering the catalytic efficiency demonstrated by each catalyst in the different tested combinations, it was decided to continue the study using only pyrite and marcasite for PMS activation under solar irradiation.

Given the catalytic efficiency demonstrated by each catalyst in the various combinations studied, we have decided to continue this investigation using pyrite and marcasite for PMS activation under solar irradiation. Consequently, specific parameters such as pH, inactivation kinetics, and the identification of reactive oxygen species (ROS) will be explored with these two catalysts before applying the system to real wastewater samples.

3.5. pH optimization

After evaluating the effects of the two catalysts, PMS, solar irradiation, and their combinations on the inactivation of *E. faecalis*, the influence of pH was investigated using the optimal conditions for the following combinations (0.05 mM of PMS and 0.25 g·L^{-1} of pyrite or marcasite). Fig. 7a and b show the inactivation efficiencies of *E. faecalis* for the two processes, respectively, across a pH range from 5 to 11 (pH values under strongly acidic and basic conditions are shown in Fig. S6 of the supplementary material).

A decrease in the *E. faecalis* inactivation efficiency was observed as pH increased, although this decrease was more gradual in the case of the PMS/Pyrite/Solar process. The observed reduction followed the order: DL, 4.65 LRV, 3.28 LRV, and 0.28 LRV for pH values of unadjusted pH, 7, 9, and 11, respectively, after 60 min of treatment. A similar trend was observed for the PMS/Marcasite/Solar process; however, the decrease in bacterial inactivation was much more pronounced and did not follow a consistent correlation with increasing pH (DL, 0.76 LRV, 0.15 LRV, and 0.80 LRV), after 30 min of treatment.

This behavior, observed for both catalysts when operating at the unadjusted pH of the reaction medium, may be linked to the surface charge of the catalysts. Therefore, the determination of the point of zero charge (pH_{zpc}) is presented in Fig. S7 (Supplementary Material). The pH_{zpc} values for pyrite and marcasite were found to be 6.21 and 6.15, respectively, indicating that at pH values below these, the catalysts carry a positive surface charge. This is the case under the unadjusted pH conditions of the system (5.50 for pyrite and 5.33 for marcasite).

Previous studies from our research group have reported that the pH_{zpc} of *E. faecalis* lies between 2 and 3 [67], suggesting a net negative charge on the bacterial surface within the studied pH range. This

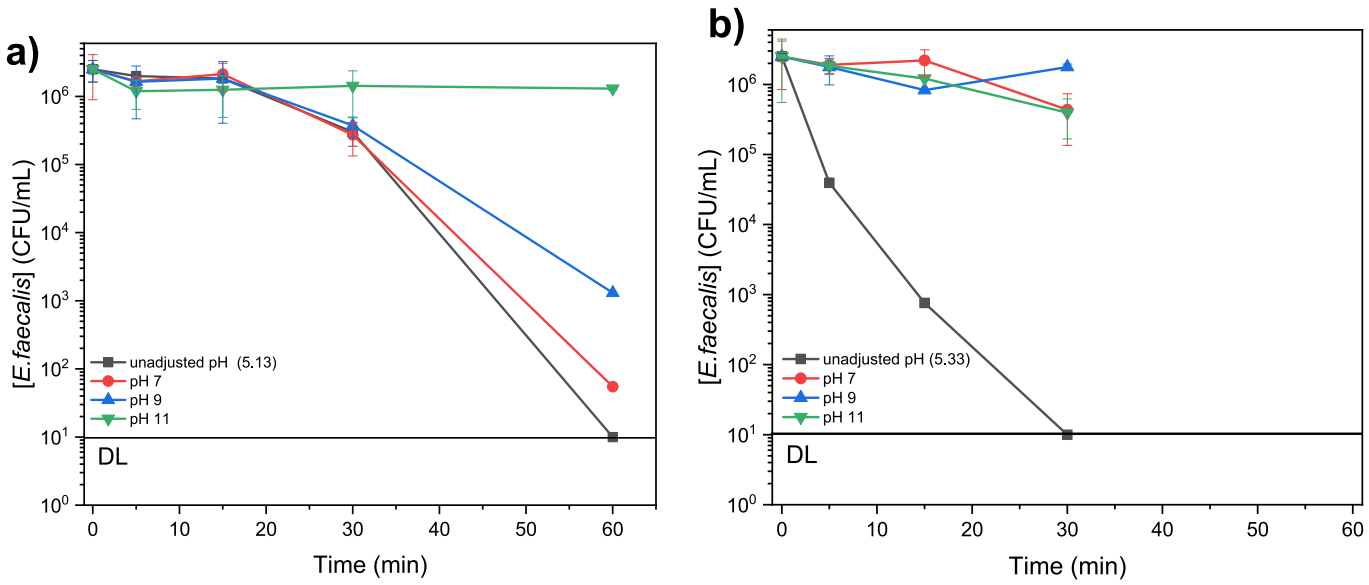

Fig. 7. Optimization of pH for the Inactivation of *E. faecalis*. (a) PMS/Pyrite/Solar, (b) PMS/Marcasite/Solar. [Pyrite] = [Marcasite] = 0.25 g·L^{-1} and [PMS] = 0.05 mM, radiation intensity 16.07 W m^{-2}.

electrostatic attraction between positively charged catalysts and negatively charged bacteria likely enhances bacterial adsorption onto the catalyst surface, thereby improving inactivation. In contrast, at pH values of 7, 9, and 11, both the catalyst and bacteria would carry negative charges, reducing this interaction and consequently lowering the efficiency.

These results suggest that both systems are more favorable for *E. faecalis* inactivation under acidic conditions. Under similar acidic and neutral conditions, Wang et al. [49–51] studied the inactivation of antibiotic-resistant bacteria through a pre-treatment with peracetic acid followed by UV irradiation. A consistent trend was observed across all their disinfection systems, indicating that a lower pH favored the inactivation of vancomycin-resistant *E. faecalis*. Specifically, with the PAA-UV/PAA system, the k_{obs} decreased from 0.683 min^{-2} under acidic conditions to 0.513 min^{-2} and 0.325 min^{-2} under neutral and alkaline conditions, respectively. The enhanced efficiency under acidic conditions was attributed to the crucial role of PAA diffusion and its effective cellular penetration during the PAA-UV/PAA process. At lower pH levels, PAA predominantly exists in its neutral molecular form, which facilitates rapid diffusion toward the negatively charged bacterial cell surfaces and promotes subsequent entry into the cells [79].

Indeed, under acidic conditions, FeS_2 can undergo oxidation, releasing Fe^{2+} ions at the surface that contribute to PMS activation, generating ROS and promoting rapid inactivation of *E. faecalis*. In alkaline environments, surface Fe^{2+} ions on pyrite and marcasite may be prematurely oxidized to Fe^{3+} before participating in PMS activation. Moreover, under basic conditions, $SO_4^{\bullet-}$ radicals derived from PMS photodecomposition can react with water molecules and hydroxide ions to form $^{\bullet}OH$, which have a lower oxidative potential (Eqs. 16 and 17 [80].

$$SO_4^{\bullet-} + H_2O \rightarrow SO_4^{2-} + OH^{\bullet} + H^{+} \quad (16)$$

$$SO_4^{\bullet-} + OH^{-} \rightarrow SO_4^{2-} + {}^{\bullet}OH \quad (17)$$

Although complete inactivation (DL) was achieved at the unadjusted pH with both catalysts, the differing trends in the decline of *E. faecalis* inactivation efficiency as pH increased suggest that pyrite is a more stable and tolerant catalyst under varying reaction conditions. This can be attributed to nature, stability, and predominance of the ROS generated in each process. Indeed, during the inactivation of *E. faecalis*, fluctuations in pH may occur, even after initial adjustment, which can significantly affect ROS generation, particularly $^{\bullet}OH$ and $O_2^{\bullet-}$ radicals. In these experiments, pH values tended to decrease over time, especially in the case of pyrite, shifting the solution toward acidic conditions close to the unadjusted pH. This observation implies that the PMS/Pyrite/Solar system may gradually self-adjust toward an acidic environment during treatment. This result highlights the buffering ability of pyrite, which enables the PMS/Pyrite/Solar system to maintain high efficiency even at pH 9, unlike marcasite. This buffering effect is likely due to the more stable oxidation of pyrite compared to marcasite, leading to the sustained release of Fe^{2+} ions and protons that lower the pH and inhibit the formation of iron-based surface precipitates [66,81]. This self-regulating capacity of mineral-based catalysts previously discussed (Eq. 12), reduces the need for external pH adjustment (acid/base) in practical applications, ultimately lowering treatment costs.

3.6. Bacterial inactivation kinetics on different processes

To better understand the contribution of each individual component within these photocatalytic PMS activation systems, and to evaluate the interactions between all elements involved, a bacterial inactivation kinetic study was conducted (Fig. S5 supplementary material). Additionally, the synergistic factors for each of the two systems were determined. Table 2 summarizes the rate constants for all combinations as well as the synergistic factors for the PMS/Pyrite/Solar and PMS/Marcasite/Solar

Table 2
Summary of calculated synergistic factors of PMS/Pyrite/Solar and PMS/Marcasite/Solar processes.

Factor	Catalyst (mg·L^{-1})	PMS (mM)	Sunlight	Catalyst	First-order constant	Synergistic index (S)
1	250			Pyrite	0.0037	
1	250			Marcasite	0.0046	
1		0.05		–	0.0002	
1			On		0.0035	
2	250		On	Pyrite	0.0484	
2	250		On	Marcasite	0.0539	
2	250	0.05		Pyrite	0.0005	
2	250	0.05		Marcasite	0.0004	
2		0.05	On		0.0327	
3	250	0.05	On	Pyrite	0.084	1.14
3	250	0.05	On	Marcasite	0.151	1.92

systems.

The synergistic factors estimated for the two respective systems were 1.14 and 1.92, both exceeding the reference value of 1, thereby confirming the presence of a synergistic interaction among the different components of the processes studied [56]. This synergy is likely due to photocatalytic reactions induced by the heterogeneous catalysts under solar irradiation, coupled with dual PMS activation: initially by sunlight and subsequently through redox reactions facilitated by electron transfer from the catalysts to PMS, an effect further enhanced by the presence of Fe^{2+} in the reaction medium. These findings suggest that the interaction among system components leads to a faster and more efficient disinfection process than any individual component alone. The photoexcitation of pyrite and marcasite under solar light likely generated electron-hole pairs (e^-/h^+), promoting PMS activation and the generation of ROS with sufficient oxidative potential to effectively attack bacterial cells. This mechanism was further supported by iron regeneration and the sustained renewal of the catalytic process through a stable Fe^{2+}/Fe^{3+} cycle in the reaction medium. Overall, this combined system, integrating chemical advanced oxidation, photocatalysis, and heterogeneous catalysis, represents a promising, sustainable, and environmentally friendly disinfection strategy.

3.7. Scavenger study

To gain deeper insight into the predominant reactive species involved in the inactivation mechanism, a scavenger study was carried out using specific radical quenchers. Moreover, previous research on mineral-based AOPs has demonstrated that pollutant removal is largely driven by reactive radical species [82]. Therefore, the contribution of each species was assessed by observing variations in inactivation efficiency following the addition of the corresponding scavenger. The results of these scavenging experiments are presented in Fig. 8a and b.

Compared to the control (without scavengers), the inactivation of *E. faecalis* in the presence of scavengers exhibited markedly different behaviors, with varying degrees of inhibition depending on the scavenger used. Specifically, the addition of MeOH led to a significant reduction in bacterial inactivation, with efficiencies dropping from 5.40 LRV (control) to 0.90 LRV and 0.08 LRV for the PMS/Pyrite/Solar and PMS/Marcasite/Solar systems, respectively. This indicates that both $SO_4^{\bullet-}$ and $^{\bullet}OH$ radicals were generated in these systems and played a key role in bacterial inactivation. The effect of TBA further highlighted the influence of hydroxyl radicals, with inactivation efficiencies decreasing to 1.13 LRV and 2.93 LRV for the pyrite and marcasite-based systems, respectively. These results suggest that $^{\bullet}OH$ radicals are involved in both processes, although the comparison with MeOH implies a more dominant role for $SO_4^{\bullet-}$ radicals, especially in the system using marcasite as the catalyst. This observation aligns with previous studies showing that while $^{\bullet}OH$ plays a crucial role, it is not necessarily the sole contributor to the overall photocatalytic activity [25–28]. To further investigate the photocatalytic activity of the two catalysts, the possible generation of other radicals was also assessed. The addition of $CHCl_3$, a scavenger for superoxide radicals ($O_2^{\bullet-}$), resulted in a notable inhibition of inactivation down to 3.60 LRV for the pyrite system and 2.13 LRV for the marcasite system. This highlights the significant, though secondary, role of $O_2^{\bullet-}$radicals in the oxidation mechanism, especially in the marcasite-based system. This finding supports the higher inactivation rate constant observed for the PMS/Marcasite/Solar system (as reported in Table S3 of the Supplementary Information), and explains the shorter time required to reach complete inactivation. In contrast, the addition of FFA, an indicator for $^1O_2$, led to only a minor inhibition, suggesting that $^1O_2$ plays a limited role in the inactivation process. Overall, these results confirm that $SO_4^{\bullet-}$, $^{\bullet}OH$ and $O_2^{\bullet-}$ radicals are the primary reactive species responsible for bacterial inactivation in the PMS/Pyrite/Solar and PMS/Marcasite/Solar systems, as illustrated in the proposed mechanisms in Fig. 9 These species act synergistically to ensure high antimicrobial performance.

3.8. Recovery and reuse of catalysts

One of the main advantages of heterogeneous catalysts over homogeneous ones, such as transition metal salts, lies in their recoverability after use. This characteristic enables the reuse of the same material in subsequent catalytic cycles, potentially lowering operational costs and making the disinfection process more suitable for continuous-flow systems. For this reason, the recovery and reuse of pyrite and marcasite in the solar-activated PMS systems were studied until a noticeable decline in inactivation efficiency was observed.

Catalyst reuse was evaluated under previously optimized conditions. After each reaction cycle, the pyrite and marcasite particles were separated from the reaction solution by centrifugation and filtration, washed three times with ultrapure water, and dried overnight in an oven before reused in the subsequent batch experiment. The results (Fig. 10a and b) show that *E. faecalis* inactivation in the PMS/Pyrite/Solar system reached DL within 60 min and remained virtually unchanged during the

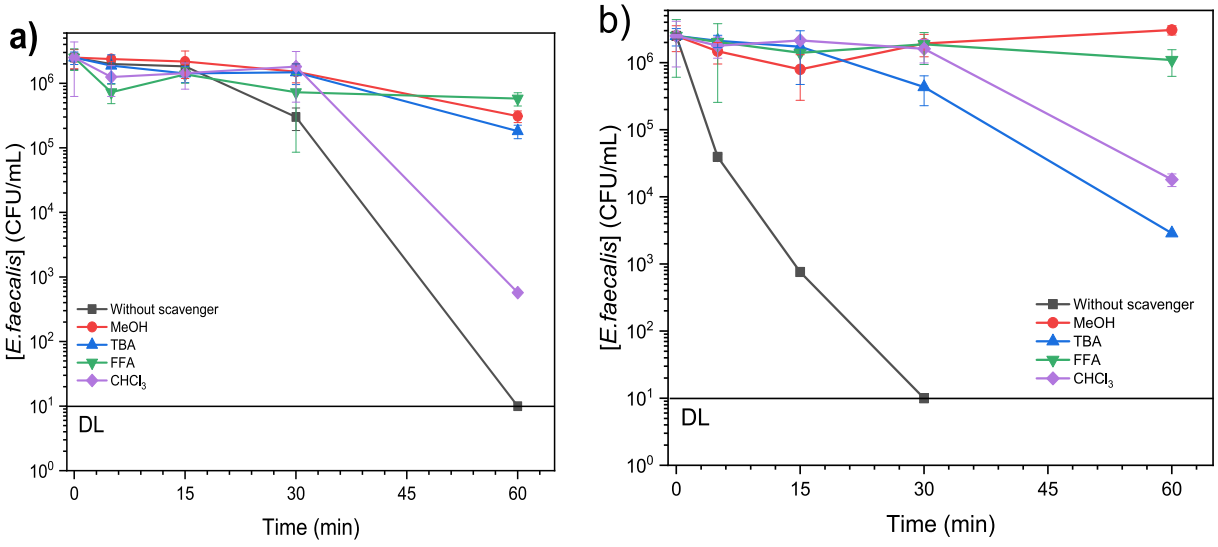

Fig. 8. Influence of quencher on *E. faecalis* inactivation in PMS/Pyrite/Solar and PMS/Marcasite/Solar system: [MeOH] = [TBA] = [FFA] = 50 mM, [$CHCl_3$] = 10 mM. [Pyrite] = [Marcasite] = 0.25 g·L^{-1} and [PMS] = 0.05 mM, radiation intensity 16.07 W m^{-2} at unadjusted pH.

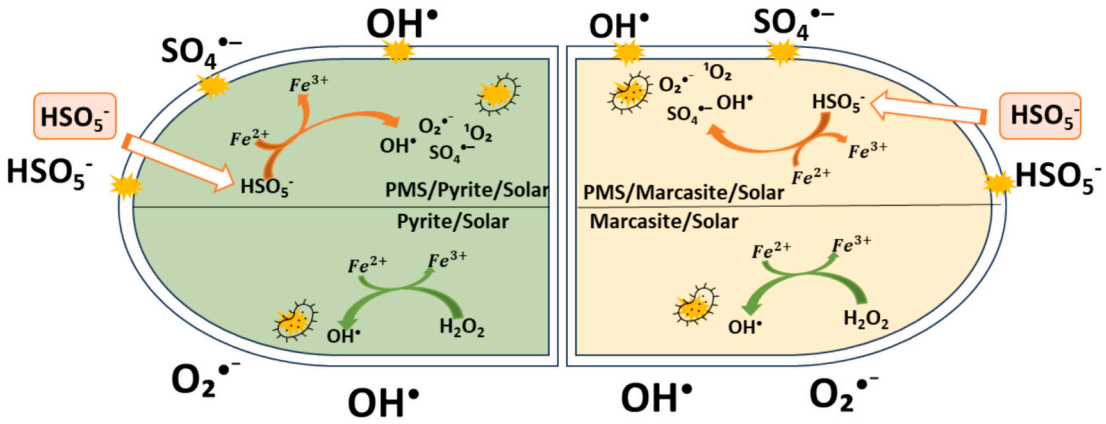

Fig. 9. Proposed mechanism for the inactivation of *E. faecalis* in the studied processes.

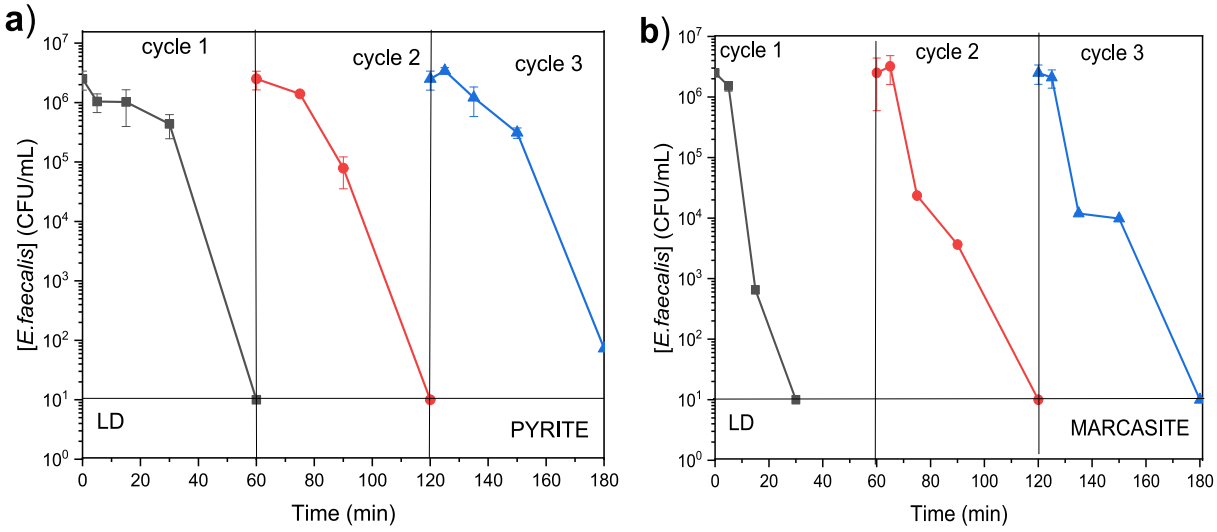

Fig. 10. The reuse performance of the PMS/Pyrite/Solar and PMS/Marcasite/Solar system in the *E. faecalis* inactivation. [Pyrite] = [Marcasite] = 0.25 g·L^{-1} and [PMS] = 0.05 mM, radiation intensity 16.07 W m^{-2} at unadjusted pH.

first reuse cycle. However, in the third cycle, inactivation efficiency dropped to 4.54 LRV, representing a 15.93 % loss after 60 min of treatment. In the PMS/Marcasite/Solar system, complete inactivation was also achieved within 30 min during the initial cycle, but efficiency dropped significantly to 2.84 LRV (47.47 % loss) and 2.40 LRV (55.46 % loss) in the second and third reuse cycles, respectively, under the same treatment duration.

It is worth noting that extending the treatment time allows the PMS/Marcasite/Solar system to recover its full disinfection efficiency, indicating that catalyst activity is not entirely lost. The gradual decrease in performance observed over reuse cycles suggests the need to further explore regeneration strategies for these catalysts. Similar findings were reported by *Lin* et al. [83], who attributed performance decline in PMS activation by pyrite to changes in surface elemental composition, which directly affect radical generation. Similarly, *Wang* et al. [22,23]. observed that the TOC_t/TOC_0 ratio decreased after each reuse cycle, with a reduction of nearly 20 % after four cycles, during their study on the heterogeneous activation of PMS by natural chalcopyrite for the efficient remediation of groundwater contaminated by aging landfill leachate. This decline was attributed to changes in the physicochemical properties of the chalcopyrite before and after the reaction. To better understand the origin of the catalytic activity decline of these materials, SEM-EDS analyses were performed after three treatment cycles to evaluate potential morphological changes and alterations in the surface elemental composition of pyrite and marcasite. The results of these analyses are presented in Figs. S8 and S9 in the Supplementary Information.

SEM images after three cycles reveal that the surfaces of both materials appear more fouled and disordered, with visible surface cracking, suggesting corrosion induced by redox reactions involved in the generation of $SO_4^{\bullet-}$ and $^{\bullet}OH$ radicals. EDS analysis of pyrite and marcasite after the third cycle showed a significant reduction in iron and sulfur content. For pyrite, Fe and S decreased from 54.96 % and 44.99 % to 46.70 % and 34.30 %, respectively. For marcasite, Fe and S decreased more dramatically, from 34.90 % and 46.09 % to 15.10 % and 12.60 %, respectively. This notable reduction in iron content suggests possible leaching of active sites during the process. It is worth noting that the compositional changes were more pronounced in the case of marcasite, which correlates with the greater decline in efficiency observed in the PMS/Marcasite/Solar system. These findings confirm that the photocatalytic activity of these materials is primarily due to the presence of surface Fe^{2+} ions, which participate in PMS activation, and S_2^{2-} species, which help sustain the Fe^{2+}/Fe^{3+} redox cycle, as previously discussed in this manuscript.

3.9. Simultaneous elimination of *E. faecalis* and tetracycline

After establishing the optimal conditions for both studied

photocatalytic systems, further experiments were conducted to assess their performance in the simultaneous removal of *E. faecalis* and a contaminant of emerging concern, tetracycline (TC). The choice of TC was based on its widespread use in treating bacterial infections in both humans and animals, and its frequent detection in environmental samples due to its poor biodegradability [84]. Recent studies have shown that approximately 75 % of administered tetracycline is excreted into the environment in either its original or partially metabolized form [85]. Because of its persistence and propensity to accumulate, TC has been associated with the development of antibiotic resistance genes and adverse health effects, including gastrointestinal symptoms (e.g., nausea and diarrhea), sore throat, and kidney complications [86]. Fig. 11a and b display the inactivation kinetics of *E. faecalis* in the presence and absence of TC. The results clearly demonstrate that the presence of TC significantly slowed the inactivation rate of *E. faecalis* in both systems. Specifically, complete inactivation was achieved in 60 min and 30 min for the PMS/Pyrite/Solar and PMS/Marcasite/Solar systems, respectively, under normal conditions, whereas the same outcome required 120 min and 90 min when TC was present.

This behavior suggests that ROS are non-selective, and that the presence of co-existing contaminants can result in competition for these species, thereby hindering the disinfection process. Nonetheless, both systems still achieved high tetracycline removal efficiencies, 98.99 % and 88.90 % for PMS/Pyrite/Solar and PMS/Marcasite/Solar, respectively, within just 30 min. This indicates that ROS may have a higher affinity toward TC, supporting the hypothesis that their interaction with TC interferes with *E. faecalis* inactivation. To confirm this, the PMS/Pyrite/solar and PMS/Marcasite/solar systems were applied to TC alone, in the absence of *E. faecalis*. The results demonstrated an outstanding removal efficiency, reaching 99.570 % and 99.661 % respectively within just 30 min of treatment. Compared to other systems specifically designed for TC degradation, these systems may even exhibit superior removal performance. For instance, *Kang* et al. [87] achieved 90 % TC removal using a Fe_3O_4@biochar/PDS system within 20 min, employing 0.1 $g{\cdot}L^{-1}$ catalyst and 0.20 $g{\cdot}L^{-1}$ PDS in ultrapure water. Similarly, *Xue* et al. [88]. used an S-type FeOOH/Bi_2MoO_6 heterojunction on biochar to degrade TC, achieving 97 % removal within 40 min using 100 $mg{\cdot}L^{-1}$ of photocatalyst and 5 mM H_2O_2 under visible light.

While the degradation efficiencies in this study are comparable to those reported in the literature using ultrapure water matrices, a key distinction is that our experiments were conducted in simulated wastewater and in the presence of co-contaminants. The results thus highlight the potential applicability of these systems in more complex and realistic water matrices.

3.10. Application of the systems in a real wastewater sample

Fig. 12 presents the results obtained for *E. faecalis* inactivation using the optimized treatment processes in a real wastewater sample, following secondary treatment. The PMS/Pyrite/Solar system achieved a 4.38 LRV reduction after 120 min, compared to the total inactivation in just 60 min when treating simulated wastewater. In contrast, the PMS/Marcasite/Solar system demonstrated better performance, achieving complete *E. faecalis* inactivation within 90 min in real wastewater, whereas only 30 min were needed for simulated wastewater. These findings highlight a decline in treatment efficiency when applied to real wastewater, both in terms of extended contact time and reduced inactivation performance, as well as a lower chemical oxygen demand (COD) removal (see Table S1, Supplementary Information). This decrease was particularly pronounced in the pyrite-based system.

This decrease in disinfection efficiency can be attributed to several factors related to the complexity of the real wastewater matrix. On one hand, the turbidity of the real wastewater was approximately 70 times higher than that of the simulated wastewater, indicating the presence of suspended particles capable of scattering and reducing solar radiation penetration. On the other hand, characterization of the sample revealed the presence of various microorganisms at relatively high concentrations (Table 1), which could contribute to reduced efficiency due to

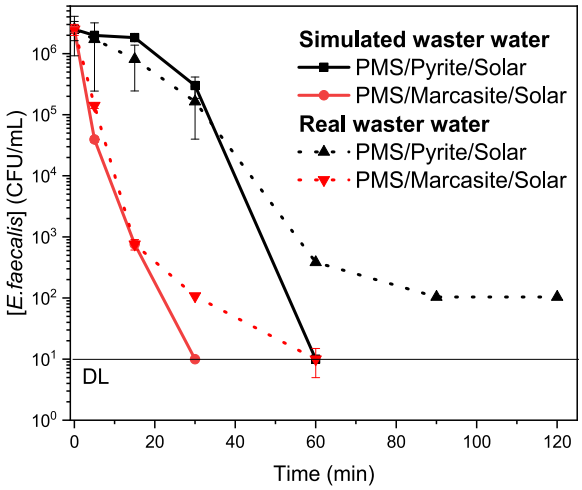

Fig. 12. Influence of the aqueous matrix on *E. faecalis* inactivation. [Pyrite] = [Marcasite] = 0.25 $g{\cdot}L^{-1}$ and [PMS] = 0.05 mM, radiation intensity 16.07 W m^{-2} at unadjasted pH.

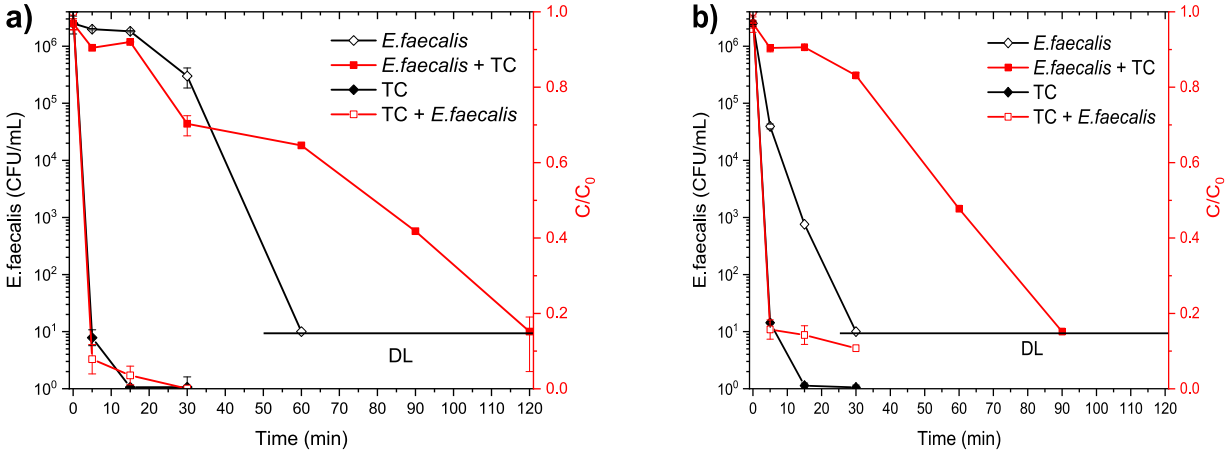

Fig. 11. Simultaneous removal of *E. faecalis* and tetracycline (TC) by the studied processes. (a) PMS/Pyrite/Solar system; (b) PMS/Marcasite/Solar system. [TC] = 10 ppm, [Pyrite] = [Marcasite] = 0.25 $g{\cdot}L^{-1}$ and [PMS] = 0.05 mM, radiation intensity 16.07 W m^{-2} at unadjusted pH.

competition among different micropollutants. Moreover, numerous studies have reported that inorganic components commonly found in real wastewater, such as carbonates, bicarbonates, nitrates, and sulfates, may negatively affect radical-based processes in certain cases [89,90]. Nevertheless, despite this decrease in performance, the tested systems still appear to be more efficient than other treatment methods applied to real wastewater. For example, *Guerra-Rodríguez* et al. [34] reported *Enterococcus* sp. inactivation levels of only 0.47 LRV and 1.41 LRV after 90 min using Sulfite/Fe(II)/UV-A and Sulfite/Fe(III)/UV-A systems, respectively over real wastewater samples. Similarly, *He* et al. [91] achieved a 2.00 LRV reduction of *E. coli* after 60 min of treatment in real wastewater using an RGO/Fe,N-TiO_2/Fe_3O_4@SiO_2 system under solar irradiation. These comparisons support the potential applicability of the systems developed in this study at a larger scale.

4. Conclusions

In this study, natural minerals were characterized and used as catalysts in a wastewater disinfection process. The minerals studied, pyrite, marcasite, and chalcopyrite, exhibited remarkable photocatalytic activity, both individually and in the presence of peroxymonosulfate (PMS) under solar irradiation, with particularly high efficiency observed for pyrite and marcasite in the inactivation of *Enterococcus faecalis*. This significant enhancement in disinfection efficiency was attributed to the generation of Fe^{2+} ions on the surface of the catalysts, which primarily promoted the production of hydroxyl radicals through photocatalysis, as well as sulfate radicals in the presence of PMS. The FeS_2 compound, present in both pyrite and marcasite, not only enabled visible light absorption under solar irradiation, but also acted as a source of photogenerated electrons and holes to activate PMS and stabilize the Fe^{2+}/Fe^{3+} redox cycle, thereby allowing continuous generation of reactive species. The determination of the energy band alignments for both minerals confirmed that they presented suitable energy band levels to perform this reaction mechanism. The PMS/pyrite/solar irradiation and PMS/marcasite/solar irradiation systems both achieved complete bacterial inactivation in less than one hour of treatment. This trend was further confirmed during the simultaneous removal of *E. faecalis* and tetracycline, resulting in total inactivation of the bacterium and respective tetracycline removal efficiencies of 98.99 and 88.90 % with the two systems. Regarding reusability, both pyrite and marcasite proved sufficient stability to be effectively recycled, due the use of a sustainable energy source. Consequently, this study highlights the promising potential of novel natural catalysts for solar-driven disinfection, and successfully demonstrates the application of photocatalysis under solar light to real wastewater samples.

CRediT authorship contribution statement

C. Gaye: Writing – review & editing, Writing – original draft, Validation, Methodology, Investigation, Formal analysis, Data curation. **P. García-Muñoz:** Writing – review & editing, Visualization, Supervision, Resources, Project administration, Funding acquisition, Formal analysis, Conceptualization. **J. Vazquez-Arenas:** Writing – review & editing, Methodology, Investigation, Formal analysis, Conceptualization. **R.H. Lara:** Methodology, Investigation, Formal analysis. **J. Rodríguez-Chueca:** Writing – review & editing, Visualization, Supervision, Resources, Project administration, Funding acquisition, Formal analysis, Conceptualization.

Declaration of Generative AI and AI-assisted technologies in the writing process

During the preparation of this work the authors used ChatGPT as AI tool for grammar and language review, which helped enhance the clarity and precision of the manuscript. After using this tool, the authors reviewed and edited the content as needed, taking full responsibility for the content of the published article.

Declaration of competing interest

The authors declare that they have no known competing financial interests or personal relationships that could have appeared to influence the work reported in this paper.

Acknowledgements

This work has received financial support from Spanish MCIN/AEI/10.13039/501100011033 and "ERDF A way of making Europe", through project PHOTORAS (PID2021-128165OA-I00). The authors gratefully acknowledge the Ministry of Higher Education, Research and Innovation, Senegal, for his mobility grant allocated to CG during this work and the support of Universidad Politécnica de Madrid. JVA appreciates financial support from SIP-IPN through Iniciación en Investigación a través de la Ejecución de Proyectos de Investigación Científica y Desarrollo Tecnológico (module 20254170).

Appendix A. Supplementary data

Supplementary data to this article can be found online at https://doi.org/10.1016/j.cej.2025.168511.

Data availability

Data will be made available on request.

References

[1] P. Pascacio, D.J. Vicente, I. Berruti, S. Nahim Granados, I. Oller, M.I. Polo-López, F. Salazar, Toward the development of an ML-driven decision support system for wastewater treatment: a bacterial inactivation prediction approach in solar photochemical processes, J. Environ. Manag. 373 (2025) 123537, https://doi.org/10.1016/j.jenvman.2024.123537.
[2] S.W. Kang, K.H. Ahn, The influence of organic matter origin on the chlorine bulk decay coefficient in reclaimed water, Water (Switzerland) 14 (5) (2022) 765, https://doi.org/10.3390/w14050765.
[3] J. Weidhaas, M. Olsen, J.E. McLean, N. Allen, L. Ahmadi, K. Duodu, R. Dupont, Microbial and chemical risk from reclaimed water use for residential irrigation, Water Reuse 12 (2022) 289–303, https://doi.org/10.2166/wrd.2022.014.
[4] S.L. Wear, V. Acuña, R. McDonald, C. Font, Sewage pollution, declining ecosystem health, and cross-sector collaboration, Biol. Conserv. 255 (2021) 109010, https://doi.org/10.1016/j.biocon.2021.109010.
[5] G. Yesilay, O.A.L. dos Santos, B.R. A, L.J. Hazeem, B.P. Backx, J.V. J, A.H. Kamel, M. Bououdina, Impact of pathogenic bacterial communities present in wastewater on aquatic organisms: application of nanomaterials for the removal of these pathogens, Aquat. Toxicol. 261 (2023) 106620, https://doi.org/10.1016/j.aquatox.2023.106620.
[6] M.M. Khalaf, H.M. Abd El-Lateef, M.F. Abo Taleb, R. Jame, M. Gouda, Encapsulation of bio-wasted derived persimmon peel extract in loaded polyvinyl alcohol/gelatin aerogel for enhanced inactivation of pathogenic bacteria in domestic sewage treatment, J. Environ. Chem. Eng. 13 (2025) 115071, https://doi.org/10.1016/j.jece.2024.115071.
[7] A. Bouriqi, N. Ouazzani, J.F. Deliège, Impact of treatment and co-treatment of different types of discharges on the improvement of receiving surface water quality, Scientific African 27 (2025) e02588, https://doi.org/10.1016/j.sciaf.2025.e02588.
[8] A. Ulusoy, A. Atılgan, R. Rolbiecki, B. Jagosz, S. Rolbiecki, Innovative approaches for sustainable wastewater resource management, Agriculture (Switzerland) 14 (12) (2024) 2111, https://doi.org/10.3390/agriculture14122111.
[9] Y. Du, Y. Yang, W.L. Wang, Y.T. Zhou, Q.Y. Wu, Surrogates for the removal by ozonation of the cytotoxicity and DNA double-strand break effects of wastewater on mammalian cells, Environ. Int. 135 (2020) 105369, https://doi.org/10.1016/j.envint.2019.105369.
[10] J. Li, Y. Sun, X. Wang, S. Xu, Changes in microbial community structures under reclaimed water replenishment conditions, Int. J. Environ. Res. Public Health 17 (4) (2020) 1174, https://doi.org/10.3390/ijerph17041174.
[11] Y. Wang, L. Serventi, Sustainability of dairy and soy processing: a review on wastewater recycling, J. Clean. Prod. 237 (2019) 117821, https://doi.org/10.1016/j.jclepro.2019.117821.
[12] A. Jodar-Abellan, M.I. López-Ortiz, J. Melgarejo-Moreno, Wastewater treatment and water reuse in Spain. Current situation and perspectives, Water (Switzerland) 11 (8) (2019) 1551, https://doi.org/10.3390/w11081551.
[13] S. Guerra-Rodríguez, E. Rodríguez, J. Rodríguez-Chueca, Pilot-scale regeneration of wastewater through intensified sulfate radical-based advanced oxidation

processes (PMS/UV-A, PMS/H2O2/UV-A, and PMS/O3): inactivation of bacteria and mechanistic considerations, Chem. Eng. J. 469 (2023) 143859, https://doi.org/10.1016/j.cej.2023.143859.
[14] X. Chen, Z. Chen, H.H. Ngo, Y. Mao, K. Cao, Q. Shi, Y. Lu, H.Y. Hu, Comparison of inactivation characteristics between Gram-positive and Gram-negative bacteria in water by synergistic UV and chlorine disinfection, Environ. Pollut. 333 (2023) 122007, https://doi.org/10.1016/j.envpol.2023.122007.
[15] A. Fiorentino, G. Ferro, M.C. Alferez, M.I. Polo-López, P. Fernández-Ibañez, L. Rizzo, Inactivation and regrowth of multidrug resistant bacteria in urban wastewater after disinfection by solar-driven and chlorination processes, J. Photochem. Photobiol. B Biol. 148 (2015) 43–50, https://doi.org/10.1016/j.jphotobiol.2015.03.029.
[16] K. Fitzhenry, E. Clifford, N. Rowan, A. Val del Rio, Bacterial inactivation, photoreactivation and dark repair post flow-through pulsed UV disinfection, J Water Process Eng 41 (2021) 102070, https://doi.org/10.1016/j.jwpe.2021.102070.
[17] C. Wang, R. Sun, R. Huang, Y. Cao, A novel strategy for enhancing heterogeneous Fenton degradation of dye wastewater using natural pyrite: kinetics and mechanism, Chemosphere 272 (2021) 129883, https://doi.org/10.1016/j.chemosphere.2021.129883.
[18] L. Wang, C. Ye, L. Guo, C. Chen, X. Kong, Y. Chen, L. Shu, P. Wang, X. Yu, J. Fang, Assessment of the UV/chlorine process in the disinfection of *Pseudomonas aeruginosa*: efficiency and mechanism, Environ. Sci. Technol. 55 (2021) 9221–9923, https://doi.org/10.1021/acs.est.1c00645.
[19] S. Zhang, L. Jiang, H. Li, J. Zhang, T. Sun, Y. Dong, N. Ding, Disinfection kinetics of peracetic acid inactivation of pathogenic bacteria in water, Water Cycle 3 (2022) 79–85, https://doi.org/10.1016/j.watcyc.2022.05.002.
[20] L. Zhu, X. Shuai, L. Xu, Y. Sun, Z. Lin, Z. Zhou, L. Meng, H. Chen, Mechanisms underlying the effect of chlorination and UV disinfection on VBNC state Escherichia coli isolated from hospital wastewater, J. Hazard. Mater. 423 (2022) 127228, https://doi.org/10.1016/j.jhazmat.2021.127228.
[21] P. García-Muñoz, C. López-Maxías, S. Guerra-Rodríguez, J. Carbajo, J.A. Casas, J. Rodríguez-Chueca, Photocatalytic activation of peroxymonosulfate using ilmenite (FeTiO3) for Enterococcus faecalis inactivation, J. Environ. Chem. Eng. 10 (2022) 108231, https://doi.org/10.1016/j.jece.2022.108231.
[22] J. Wang, L. Bu, Y. Wu, J. Sun, G. Li, S. Zhou, Disinfection profiles and mechanisms of *E. coli*, *S. aureus*, and *B. subtilis* in UV365/chlorine process: inactivation, reactivation, and DBP formation, Sep. Purif. Technol. 287 (2022) 120584, https://doi.org/10.1016/j.seppur.2022.120584.
[23] H. Wang, B. Liao, M. Hu, Y. Ai, L. Wen, S. Yang, Z. Ye, J. Qin, G. Liu, Heterogeneous activation of peroxymonosulfate by natural chalcopyrite for efficient remediation of groundwater polluted by aged landfill leachate, Appl. Catal. B Environ. 300 (2022) 120744, https://doi.org/10.1016/j.apcatb.2021.120744.
[24] J. Zheng, C. Su, J. Zhou, L. Xu, Y. Qian, H. Chen, Effects and mechanisms of ultraviolet, chlorination, and ozone disinfection on antibiotic resistance genes in secondary effluents of municipal wastewater treatment plants, Chem. Eng. J. 317 (2017) 309–316, https://doi.org/10.1016/j.cej.2017.02.076.
[25] Q. Wang, J. Gao, H. Chen, Y. Liu, X. Fu, Inactivation of Gram-positive and Gram-negative resistant bacteria by pyrite-activated dual oxidant system of peroxymonosulfate and sodium percarbonate, Sep. Purif. Technol. 364 (2025) 132463, https://doi.org/10.1016/j.seppur.2025.132463.
[26] Y. Wang, S. Wang, Y. Liu, J. Wang, Visible light-enhanced interface interaction for PMS activation towards the removal of emerging organic pollutants: performance, mechanism and toxicity, Sep. Purif. Technol. 354 (2025) 128741, https://doi.org/10.1016/j.seppur.2024.128741.
[27] Z. Wang, J. Xiong, J. Zhou, Z. Han, Algae removal and degradation of microcystins by UV-C system: a review, Water Environ. Res. 97 (3) (2025) e70049, https://doi.org/10.1002/wer.70049.
[28] S. Wang, Z. Yang, Z. Hu, C. Li, F. Yang, M. Zhang, D. Yu, M. Wu, B. Yu, Crystal-dependent doping effects over MnO2 for Fenton-like catalysis optimization, Sep. Purif. Technol. 355 (2025) 129783, https://doi.org/10.1016/j.seppur.2024.129783.
[29] L. Rizzo, W. Gernjak, P. Krzeminski, S. Malato, C.S. McArdell, J.A.S. Perez, H. Schaar, D. Fatta-Kassinos, Best available technologies and treatment trains to address current challenges in urban wastewater reuse for irrigation of crops in EU countries, Sci. Total Environ. 710 (2020) 136312, https://doi.org/10.1016/j.scitotenv.2019.136312.
[30] P. Ozores Diez, S. Giannakis, J. Rodríguez-Chueca, D. Wang, B. Quilty, R. Devery, K. McGuigan, C. Pulgarin, Enhancing solar disinfection (SODIS) with the photo-Fenton or the Fe2+/peroxymonosulfate-activation process in large-scale plastic bottles leads to toxicologically safe drinking water, Water Res. 186 (2020) 116387, https://doi.org/10.1016/j.watres.2020.116387.
[31] C. Gaye, J. Rodríguez-Chueca, A. Ortíz Fuduo, M. Fall, P. García-Muñoz, Upcycling Guiera Senegalensis waste into biochar for sustainable amoxicillin removal from water, J Water Process Eng 73 (2025) 107726, https://doi.org/10.1016/j.jwpe.2025.107726.
[32] I. Ahmad, M. Kedhim, Y. Jadeja, G. Sangwan, V. Kavitha, A. Kashyap, S. Shomurotova, M. Kazemi, R. Javahershenas, A comprehensive review on carbonylation reactions: catalysis by magnetic nanoparticle-supported transition metals, in: Nanoscale Advances 7, Royal Society of Chemistry, 2025, pp. 3189–3209, https://doi.org/10.1039/d5na00040h.
[33] N. Zhang, W. He, Z. Cheng, J. Lu, Y. Zhou, D. Ding, S. Rong, Construction of α-MnO2/g-C3N4 Z-scheme heterojunction for photothermal synergistic catalytic decomposition of formaldehyde, Chem. Eng. J. 466 (2023) 143160, https://doi.org/10.1016/j.cej.2023.143160.
[34] S. Guerra-Rodríguez, N. Cediel, E. Rodríguez, J. Rodríguez-Chueca, Photocatalytic activation of sulfite using Fe(II) and Fe(III) for Enterococcus sp. inactivation in urban wastewater, Chem. Eng. J. 408 (2021), https://doi.org/10.1016/j.cej.2020.127326.
[35] Z. Honarmandrad, X. Sun, Z. Wang, M. Naushad, G. Boczkaj, Activated persulfate and peroxymonosulfate based advanced oxidation processes (AOPs) for antibiotics degradation - A review, in: Water Resources and Industry 29, Elsevier B.V., 2023 100194, https://doi.org/10.1016/j.wri.2022.100194.
[36] N. López-Vinent, A. Cruz-Alcalde, G. Moussavi, I. del Castillo Gonzalez, A. Hernandez Lehmann, J. Giménez, S. Giannakis, Improving ferrate disinfection and decontamination performance at neutral pH by activating peroxymonosulfate under solar light, Chem. Eng. J. 450 (2022) 137904, https://doi.org/10.1016/j.cej.2022.137904.
[37] S. Miralles-Cuevas, D. Darowna, A. Wanag, S. Mozia, S. Malato, I. Oller, Comparison of UV/H_2O_2, UV/$S_2O_8^{2-}$, solar/Fe(II)/H_2O_2 and solar/Fe(II)/$S_2O_8^{2-}$ at pilot plant scale for the elimination of micro-contaminants in natural water: an economic assessment, Chem. Eng. J. 310 (2017) 514–524, https://doi.org/10.1016/j.cej.2016.06.121.
[38] J. Jia, M. Minella, M.C. Ruiz, J. Decker, D. Li, N.P.F. Gonçalves, A.B. Prevot, T. Lin, S. Giannakis, Small concentrations, big results: μM addition of photoactive iron oxides with PMS, PDS, or H2O2, leads to enhanced removal of viruses at near-neutral pH, Water Res. 258 (2024) 121760, https://doi.org/10.1016/j.watres.2024.121760.
[39] H. Liu, J. Yan, Y. Wu, C. Yan, M. Nie, W. Dong, Comparative study of Fe(III)/peroxymonosulfate, Fe(III)/hydrogen peroxide and Fe(III)/peroxydisulfate systems modified by sinapic acid for micropollutants degradation, J. Clean. Prod. 470 (2024) 143242, https://doi.org/10.1016/j.jclepro.2024.143242.
[40] W. He, L. Huang, X. Wang, J. Zhang, Molybdenum nitride(γ-Mo2N) as a novel co-catalyst to enhance Fe(III)/Fe(II) cycle for homogeneous and heterogeneous peroxymonosulfate activation: performance and mechanism, J. Environ. Chem. Eng. 12 (2024) 112404, https://doi.org/10.1016/j.jece.2024.112404.
[41] C.H. Mak, X. Han, M. Du, J.J. Kai, K.F. Tsang, G. Jia, K.C. Cheng, H.H. Shen, H. Y. Hsu, Heterogenization of homogeneous photocatalysts utilizing synthetic and natural support materials, in: Journal of Materials Chemistry A 9(8), Royal Society of Chemistry, 2021, pp. 4454–4504, https://doi.org/10.1039/d0ta08334h.
[42] M. Sohail, S. Rauf, M. Irfan, A. Hayat, M.M. Alghamdi, A.A. El-Zahhar, D. Ghernaout, Y. Al-Hadeethi, W. Lv, Recent developments, advances and strategies in heterogeneous photocatalysts for water splitting, in: Nanoscale Advances 6, Royal Society of Chemistry, 2024, pp. 1286–1330, https://doi.org/10.1039/d3na00442b.
[43] A. Yadollahi, H. Abdollahi, F.D. Ardejani, M. Mirmohammadi, S. Magdouli, Bio-oxidation behavior of pyrite, marcasite, pyrrhotite, and arsenopyrite by sulfur- and iron-oxidizing acidophiles, Bioresour Technol Rep. 15 (2021) 100699, https://doi.org/10.1016/j.biteb.2021.100699.
[44] X. Chen, N. Zhao, X. Hu, A novel strategy of pulsed electro-assisted pyrite activation of peroxymonosulfate for the degradation of tetracycline hydrochloride, Sep. Purif. Technol. 280 (2022) 119781, https://doi.org/10.1016/j.seppur.2021.119781.
[45] L. Labiadh, S. Ammar, A.R. Kamali, Oxidation/mineralization of AO7 by electro-Fenton process using chalcopyrite as the heterogeneous source of iron and copper catalysts with enhanced degradation activity and reusability, J. Electroanal. Chem. 853 (2019) 113532, https://doi.org/10.1016/j.jelechem.2019.113532.
[46] X. Zhang, H. Deng, G. Zhang, F. Yang, G.E. Yuan, Natural bornite as an efficient and cost-effective persulfate activator for degradation of tetracycline: performance and mechanism, Chem. Eng. J. 381 (2020) 122717, https://doi.org/10.1016/j.cej.2019.122717.
[47] Y. Li, H. Dong, L. Li, J. Xiao, S. Xiao, Z. Jin, Efficient degradation of sulfamethazine via activation of percarbonate by chalcopyrite, Water Res. 202 (2021) 117451, https://doi.org/10.1016/j.watres.2021.117451.
[48] R. Zheng, J. Li, R. Zhu, R. Wang, X. Feng, Z. Chen, W. Wei, D. Yang, H. Chen, Enhanced Cr(VI) reduction on natural chalcopyrite mineral modulated by degradation intermediates of RhB, J. Hazard. Mater. 423 (2022) 127206, https://doi.org/10.1016/j.jhazmat.2021.127206.
[49] Z. Wang, Y. Huang, M. Yu, W. Zhuang, M. Sui, Pre-exposure to peracetic acid followed by UV treatment for deactivating vancomycin-resistant Enterococcus faecalis through intracellular attack, Environ. Res. 262 (2024) 119780, https://doi.org/10.1016/j.envres.2024.119780.
[50] K. Wang, H. Li, W. Yu, T. Ma, Insights into structural and functional regulation of chalcopyrite and enhanced mechanism of reactive oxygen species (ROS) generation in advanced oxidation process (AOP): a review, Sci. Total Environ. 919 (2024) 170530, https://doi.org/10.1016/j.scitotenv.2024.170530.
[51] C. Wang, H. Liu, X. Li, Y. Cao, K. Jia, Degradation of organic pollutants in natural magnetite-activated peroxymonosulfate system enhanced by hydroxylamine: catalytic performance, reaction pathway, and enhancement mechanism, J Water Process Eng 66 (2024) 106000, https://doi.org/10.1016/j.jwpe.2024.106000.
[52] S. Zhu, Z. Li, M. Yu, Q. Wang, C. Chen, J. Ma, Efficient removal of naphthenic acids from real petroleum wastewater by natural pyrite activated persulfate system, J. Environ. Manag. 348 (2023) 119239, https://doi.org/10.1016/j.jenvman.2023.119239.
[53] J. Yuan, Y. Li, Z. Ding, A. Yu, X. Gong, S. Wen, S. Bai, Heterogeneous activation of peroxymonosulfate by natural chalcopyrite for degradation of ammonium dibutyl dithiophosphate from mineral processing wastewater, Sep. Purif. Technol. 341 (2024) 126741, https://doi.org/10.1016/j.seppur.2024.126741.
[54] D. Haro, P. García-Muñoz, M. Mola, F. Fresno, J. Rodríguez-Chueca, Atacamite (Cu2Cl(OH)3) as catalyst of different AOPs for water disinfection, Catal. Today 429 (2024) 114496, https://doi.org/10.1016/j.cattod.2023.114496.

[55] J. Rodríguez-Chueca, E. Barahona-García, V. Blanco-Gutiérrez, L. Isidoro-García, A.J. Dos santos-García, Magnetic CoFe2O4 ferrite for peroxymonosulfate activation for disinfection of wastewater, Chem. Eng. J. 398 (2020) 125606, https://doi.org/10.1016/j.cej.2020.125606.
[56] S. Guerra-Rodríguez, E. Rodríguez, J. Moreno-Andrés, J. Rodríguez-Chueca, Effect of the water matrix and reactor configuration on Enterococcus sp. inactivation by UV-A activated PMS or H2O2, J. Water Process Eng. 47 (2022) 102740, https://doi.org/10.1016/j.jwpe.2022.102740.
[57] T. Danesh, T. Hsia, C. Ritchie, S.H. Thang, Flotation efficiency and surface adsorption mechanism on chalcopyrite and pyrite by a novel cardanol derivative 3-pentadecylphenyl 4-(3,3-diethylthiouredo-4-oxobutanoate), Miner. Eng. 207 (2024) 108566, https://doi.org/10.1016/j.mineng.2023.108566.
[58] N. Liao, C. Wu, J. Xu, B. Feng, J. Wu, Y. Gong, Effect of grinding media on grinding-flotation behavior of chalcopyrite and pyrite, Front. Mater. 7 (2020), https://doi.org/10.3389/fmats.2020.00176.
[59] S.S. Mohammed Ameen, D.D. Hassan, D.S. Mohammed, K.M. Omer, D.A. Latif, Y. O. Mohammad, Natural-based chalcopyrite nanoparticles as high-performance mineral adsorbents for organic dye removal in water, Mater. Adv. 6 (2025) 2192–2201, https://doi.org/10.1039/d5ma00038f.
[60] Domè, C., De Pablo, J., & Ayora, C. (n.d.). Oxidative dissolution of pyritic sludge from the Aznalcóllar mine (SW Spain). www.elsevier.com/locate/chemgeo.
[61] S. Macchi, M. Nemer, M.M. Mills, M.L. Meyerson, H.W. Papenguth, J.H. Taphouse, N.B. Schorr, Comparing methods for pyrite surface area measurement through optical, aqueous, and gaseous approaches, Sci 7 (1) (2025) 8, https://doi.org/10.3390/sci7010008.
[62] G.H. Kelsall, Q. Yin, D.J. Vaughan, K.E.R. England, N.P. Brandon, Electrochemical oxidation of pyrite (FeS2) in aqueous electrolytes, J. Electroanal. Chem. 471 (2) (1999) 116–125.
[63] Y. Lin, J. Li, S. Chen, H. Zhou, Y. Shu, L. Tang, Q. Long, P. Zhang, Y. Huang, In situ construction of pyrite-marcasite-magnetite composite via FeS2 phase transformation and oxidation for the synergistic degradation of methyl orange and Cr(VI), Sep. Purif. Technol. 308 (2023) 122764, https://doi.org/10.1016/j.seppur.2022.122764.
[64] T.K. Trinh, V.T.H. Pham, N.T.N. Truong, C.D. Kim, C. Park, Iron pyrite: phase and shape control by facile hot injection method, J. Cryst. Growth 461 (2017) 53–59, https://doi.org/10.1016/j.jcrysgro.2016.12.108.
[65] A. Zaka, S.M. Alhassan, A. Nayfeh, Iron pyrite in photovoltaics: a review on recent trends and challenges, in: ACS Applied Electronic Materials 4, American Chemical Society, 2022, pp. 4173–4211, https://doi.org/10.1021/acsaelm.2c00489.
[66] Y. Liang, Z. Tu, Q. Wu, X. Zhang, X. Tan, X. Guan, J. Zhao, Degradation of printing and dyeing wastewater pollutant reactive black 5 via pyrite activated persulfate: efficacy and application impact assessment, J Water Process Eng 70 (2025) 107082, https://doi.org/10.1016/j.jwpe.2025.107082.
[67] P. García-Muñoz, E. Gatica, G. Dos Santos Teixeira, D. Contreras, J. Rodríguez-Chueca, Do Fe2O3/TiO2 heterojunctions improve the wastewater disinfection process? J. Environ. Manag. 373 (2025) 123773 https://doi.org/10.1016/j.jenvman.2024.123773.
[68] R. Sun, M.K.Y. Chan, G. Ceder, First-principles electronic structure and relative stability of pyrite and marcasite: implications for photovoltaic performance, Phys. Rev. B - Condens. Matter Mater. Phys. 83 (2011) 235311, https://doi.org/10.1103/PhysRevB.83.235311.
[69] Q. Zhang, J. Li, Y. Li, L. Zhang, S. Zhong, X. Ru, X. Shu, Investigation into the synergistic roles of exposed crystal planes and S vacancies during the photo-Fenton degradation of sulfadiazine via pyrite with three different morphologies, Sep. Purif. Technol. 353 (2025) 128538, https://doi.org/10.1016/j.seppur.2024.128538.
[70] J. Rodríguez-Chueca, S. Giannakis, M. Marjanovic, M. Kohantorabi, M.R. Gholami, D. Grandjean, L.F. de Alencastro, C. Pulgarín, Solar-assisted bacterial disinfection and removal of contaminants of emerging concern by Fe2+-activated HSO5- vs. S2O82- in drinking water, Appl. Catal. B Environ. 248 (2019) 62–72, https://doi.org/10.1016/j.apcatb.2019.02.018.
[71] J. Du, C. Wang, M. Sun, G. Chen, C. Liu, X. Deng, R. Chen, Z. Zhao, Novel vacuum UV/ozone/peroxymonosulfate process for efficient degradation of levofloxacin: performance evaluation and mechanism insight, J. Hazard. Mater. 463 (2024) 132916, https://doi.org/10.1016/j.jhazmat.2023.132916.
[72] P. Saraç Uluçtan, H. Atalay Eroğlu, E. Nihan Kadıoğlu, F. Akbal, Decolorization of Acid Red 337 dye with hydroxyl and sulfate radical based advanced oxidation processes using different iron catalyst: an experimental and statistical investigation, J. Photochem. Photobiol. A Chem. 459 (2025) 116105, https://doi.org/10.1016/j.jphotochem.2024.116105.
[73] Q. Shen, X. Song, J. Fan, C. Chen, Z. Guo, Degradation of humic acid by UV/PMS: process comparison, influencing factors, and degradation mechanism, RSC Adv. 14 (2024) 22988–23003, https://doi.org/10.1039/d4ra04328f.
[74] N. Zhang, J. Li, H. Wu, H. Lv, H. Zhao, F. Cheng, Efficient removal of bisphenol A by carbon nitride/peroxymonosulfate/solar system: multi-radical association mechanism by the morphology and crystallinity optimization, React. Kinet. Mech. Catal. 137 (2024) 1015–1030, https://doi.org/10.1007/s11144-024-02566-5.
[75] S. Xiao, M. Cheng, H. Zhong, Z. Liu, Y. Liu, X. Yang, Q. Liang, Iron-mediated activation of persulfate and peroxymonosulfate in both homogeneous and heterogeneous ways: a review, Chem. Eng. J. 384 (2020) 123265, https://doi.org/10.1016/j.cej.2019.123265.
[76] D. Kim, K. Yong, Boron doping induced charge transfer switching of a C3N4/ZnO photocatalyst from Z-scheme to type II to enhance photocatalytic hydrogen production, Appl. Catal. B Environ. 282 (2021) 119538, https://doi.org/10.1016/j.apcatb.2020.119538.
[77] Y. Bai, W. Wang, F. Xie, D. Lu, K. Jiang, D. Dreisinger, In-situ electrochemical study of chalcopyrite pressure oxidation leaching from 110 °C to 150 °C under saturated vapor pressure, Arab. J. Chem. 15 (2022) 104139, https://doi.org/10.1016/j.arabjc.2022.104139.
[78] N. Barhoumi, H. Olvera-Vargas, N. Oturan, D. Huguenot, A. Gadri, S. Ammar, E. Brillas, M.A. Oturan, Kinetics of oxidative degradation/mineralization pathways of the antibiotic tetracycline by the novel heterogeneous electro-Fenton process with solid catalyst chalcopyrite, Appl. Catal. B Environ. 209 (2017) 637–647, https://doi.org/10.1016/j.apcatb.2017.03.034.
[79] M. Lavoie, S. Le Faucheur, A. Boullemant, C. Fortin, P.G.C. Campbell, The influence of pH on algal cell membrane permeability and its implications for the uptake of lipophilic metal complexes, J. Phycol. 48 (2012) 293–302, https://doi.org/10.1111/j.1529-8817.2012.01126.x.
[80] Z. Tu, Y. Liang, S. Zhou, X. Zhang, X. Tan, G. Yu, X. Zhang, J.R. Reinfelder, Application of pyrite to water pollutant removal: a review, J. Water Process Eng. 68 (2024) 106375, https://doi.org/10.1016/j.jwpe.2024.106375.
[81] S. Peng, Y. Feng, Y. Liu, D. Wu, Applicability study on the degradation of acetaminophen via an H2O2/PDS-based advanced oxidation process using pyrite, Chemosphere 212 (2018) 438–446, https://doi.org/10.1016/j.chemosphere.2018.08.023.
[82] Y. Wu, Y. Li, H. Zhang, H. Wang, Application of natural mineral materials in advanced oxidation processes for wastewater treatment: a review, J. Environ. Chem. Eng. 12 (2024) 111885, https://doi.org/10.1016/j.jece.2024.111885.
[83] X. Lin, J. Hu, Z. Mo, Z. Wang, R. Wang, J. Liang, pH-dependent mechanisms of sulfadiazine degradation by natural pyrite-driven heterogeneous Fenton-like reactions, J. Environ. Manag. 365 (2024) 121607, https://doi.org/10.1016/j.jenvman.2024.121607.
[84] H. Li, C. Liu, Z. Mou, P. Yu, S. Wu, W. Wang, Z. Wang, R. Yuan, Enhancement of peroxymonosulfate activation with nickel foam-supported CuCo2O4 for tetracycline degradation: performance and mechanism insights, J. Colloid Interface Sci. 678 (2025) 227–241, https://doi.org/10.1016/j.jcis.2024.09.104.
[85] S.V. Lundström, M. Östman, J. Bengtsson-Palme, C. Rutgersson, M. Thoudal, T. Sircar, H. Blanck, K.M. Eriksson, M. Tysklind, C.F. Flach, D.G.J. Larsson, Minimal selective concentrations of tetracycline in complex aquatic bacterial biofilms, Sci. Total Environ. 553 (2016) 587–595, https://doi.org/10.1016/j.scitotenv.2016.02.103.
[86] P.A. Taksal, S. Arasavilli, B.K. Das, K. Ray, S. Chowdhury, J. Bhattacharya, Green graphitic-carbon bridged Ag2S/g-C3N4 S-scheme photocatalyst for tetracycline degradation in water with antimicrobial activity: from synthesis to commercialization prospect, Sep. Purif. Technol. 361 (2025) 131610, https://doi.org/10.1016/j.seppur.2025.131610.
[87] H. Kang, H. Ren, A. Labidi, Y. Liao, Y. Wang, H. Zheng, D. Bahnemann, C. Wang, Fe3O4 loaded biochar to enhance persulfate activation for tetracycline degradation: performance and mechanism, Chemosphere 376 (2025) 144267, https://doi.org/10.1016/j.chemosphere.2025.144267.
[88] Q. Xue, H. Lin, Q. Feng, Y. Yang, M. Dong, K. Hu, B. Song, P. Sean Goh, X. Shen, Synergistic photocatalysis and Fenton-like process driven by a biochar-supported biochar/iron hydroxide oxide/bismuth molybdate S-type heterojunction for tetracycline degradation: mechanistic insights and degradation pathways, Appl. Surf. Sci. 679 (2025) 161277, https://doi.org/10.1016/j.apsusc.2024.161277.
[89] L. Sbardella, I. Velo-Gala, J. Comas, I. Rodríguez-Roda Layret, A. Fenu, W. Gernjak, The impact of wastewater matrix on the degradation of pharmaceutically active compounds by oxidation processes including ultraviolet radiation and sulfate radicals, J. Hazard. Mater. 380 (2019) 120869, https://doi.org/10.1016/j.jhazmat.2019.120869.
[90] S. Wacławek, H.V. Lutze, K. Grübel, V.V.T. Padil, M. Černík, D.D. Dionysiou, Chemistry of persulfates in water and wastewater treatment: a review, Chem. Eng. J. 330 (2017) 44–62, https://doi.org/10.1016/j.cej.2017.07.132.
[91] J. He, Z. Zheng, I.M.C. Lo, Different responses of gram-negative and gram-positive bacteria to photocatalytic disinfection using solar-light-driven magnetic TiO2-based material, and disinfection of real sewage, Water Res. 207 (2021) 117816, https://doi.org/10.1016/j.watres.2021.117816.